Available online at www.sciencedirect.com
SCIENCE DIRECT®
Comput. Methods Appl. Mech. Engrg. 195 (2006) 2334–2370
Computer methods in applied mechanics and engineering
www.elsevier.com/locate/cma

Co-rotational finite element formulation for thin-walled beams with generic open section

Hong Hu Chen [a], Wen Yi Lin [b], Kuo Mo Hsiao [a,*]

[a] Department of Mechanical Engineering, National Chiao Tung University, 1001 Ta Hsueh Road, Hsinchu, Taiwan, ROC
[b] Department of Mechanical Engineering, De Lin Institute of Technology, 1 Alley 380, Ching Yun Road, Tucheng, Taiwan, ROC

Received 11 February 2004; received in revised form 18 March 2005; accepted 13 May 2005

Abstract

A consistent co-rotational total Lagrangian finite element formulation for the geometric nonlinear buckling and postbuckling analysis of thin-walled beams with generic open section is presented. The element developed here has two nodes with seven degrees of freedom per node. The element nodes are chosen to be located at the shear centers of the end cross-sections of the beam element and the shear center axis is chosen to be the reference axis. The deformations of the beam element are described in the current element coordinate system constructed at the current configuration of the beam element. The element nodal forces are derived using the virtual work principle. The virtual rigid body motion corresponding to the virtual nodal displacements is excluded in the derivation of the element nodal forces. A procedure is proposed to determine the virtual rigid body motion. The way used to determine the element coordinate system and element nodal deformations corresponding to the virtual nodal displacements and that corresponding to the incremental nodal displacement are consistent. In element nodal forces, all coupling among bending, twisting, and stretching deformations of the beam element is considered by consistent second-order linearization of the fully geometrically nonlinear beam theory. In the derivation of the element tangent stiffness matrix, the change of element nodal forces induced by the element rigid body rotations should be considered for the present method. Thus, a stability matrix is included in the element tangent stiffness matrix. An incremental-iterative method based on the Newton–Raphson method combined with constant arc length of incremental displacement vector is employed for the solution of nonlinear equilibrium equations. The zero value of the tangent stiffness matrix determinant of the structure is used as the criterion of the buckling state. Numerical examples are presented to investigate the accuracy and efficiency of the proposed method. The effect of the terms in the element nodal force and tangent stiffness matrix, which will converge to zero with the decrease of element size, on the convergence rate of solution and accuracy for the buckling load and nonlinear behavior of three dimensional beam structures are also investigated through numerical examples.

* Corresponding author. Fax: +886 35 720 634.
E-mail address: kmhsiao@cc.nctu.edu.tw (K.M. Hsiao).

0045-7825/$ - see front matter © 2005 Elsevier B.V. All rights reserved.
doi:10.1016/j.cma.2005.05.011

Keywords: Co-rotational formulation; Thin-walled beam; Geometric nonlinearity; Buckling

1. Introduction

Due to reduction of weight, material and cost, thin-walled beams with open section are extensively used in aerospace and aircraft structures, and are often designed to work under postbuckling conditions. Such flexible structures can undergo large displacements and rotations without exceeding their elastic limits. To understand the behaviors of such flexible structures and to evaluate their elastic limits many different formulations and numerical procedures for the buckling and postbuckling analysis of thin-walled beams have been proposed [1–42]. The buckling of the beam structures is caused by the coupling among bending, twisting, and stretching deformations of the beam members. Thus the buckling analysis is a subtopic of nonlinear rather than linear mechanics [8]. Currently, the most popular approach for the analysis of three-dimensional beam is to develop finite element models. The formulations, which have been used in the literature, might be divided into three categories [43]: total Lagrangian (TL) formulation, updated Lagrangian (UL) formulation, and co-rotational (CR) formulation. In order to capture correctly all coupling among bending, twisting, and stretching deformations of the beam elements, the formulation of beam elements might be derived by the fully geometrically nonlinear beam theory [44]. The exact expressions for the element nodal forces, which are required in a TL formulation for large displacement/small strain problems, are highly nonlinear functions of element nodal parameters. However, the dominant factors in the geometrical nonlinearities of beam structures are attributable to finite rotations, the strains remaining small. For a beam structure discretized by finite elements, this implies that the motion of the individual elements to a large extent will consist of rigid body motion. If the rigid body motion part is eliminated from the total displacements and the element size is properly chosen, the deformational part of the motion is always small relative to the local element axes. Thus in conjunction with the CR formulation, the higher order terms of nodal parameters in the element nodal forces may be neglected by consistent second order linearization [24,44]. In [38], Hsiao and Lin presented a co-rotational total Lagrangian formulation of beam element for the nonlinear analysis of monosymmetric thin-walled open-section beams with large rotations but small strains. In [38], the bimoment [45,46] was considered to be a generalized nodal force and the twist rate to be the associated generalized nodal displacement. The beam element had 2 nodes with seven degrees of freedom per node. Element deformations and element equations were defined in terms of element coordinates, which were constructed at the current configuration of the beam element. The element deformations were determined by the rotation of element cross-section coordinates, which were rigidly tied to element cross-section, relative to the element coordinate system [24]. The formulation of element nodal forces was derived by consistent second-order linearization of the fully geometrically nonlinear beam theory. However, the third order term of the twist rate is retained in the element nodal forces as suggested by [36,37]. This element was proven to be very effective for geometric nonlinear analysis of three dimensional beams by numerical examples studied in [38]. However, the beam element cannot be used for the analysis of thin-walled beams with asymmetric open section. To the authors' knowledge, the application of co-rotational formulation in the geometric nonlinear buckling and postbuckling analysis for thin-walled beams with generic open section is rather rare in the literature. In [39], based on semitangential concept, an updated Lagrangian co-rotational formulation was developed for geometrically nonlinear analysis of asymmetric thin-walled frames. In the iterative evaluation, total element forces are accumulated from incremental element forces. In [40], a formulation of 3D co-rotational beam elements for the nonlinear and stability analysis of frame structures was proposed. It seems that the formulation proposed in [40] can be applied to the asymmetric

thin-walled frames. However, no numerical example of thin-walled frames with asymmetric cross-section was studied in [40]. The object of this paper is to present a consistent co-rotational total Lagrangian finite element formulation for the geometric nonlinear buckling and postbuckling analysis of thin-walled beams with generic open section.

Here, the kinematic assumptions made in [38] are used. Following [38], the shear center axis is chosen to be the reference axis and the element nodes are chosen to be located at the shear centers of the end cross-sections of the beam element. In [24], a procedure was proposed is to determine the current element coordinates and current element nodal rotation parameters corresponding to a given incremental nodal displacements and rotations. The deformations, internal nodal forces and stiffness matrix of the elements are defined in terms of these coordinates. This method was employed in [34,36–38,41]. In [24], the element virtual rigid body motions are not excluded from the corresponding virtual element nodal displacements and rotations. Thus, the method proposed in [24] may be regarded as generalized co-rotational formulation. In this paper, a consistent co-rotation formulation will be used. A procedure will be proposed to remove the element virtual rigid body motions and determine the element virtual nodal deformation. The new configuration corresponding to the virtual element nodal displacements and rotations is referred to as the virtual displaced configuration here. The element coordinates and nodal rotation parameters corresponding to the virtual displaced configuration are determined by the method described in [24] and the consistent first order linearization. The difference between the nodal rotation parameters and the difference between the chord length of the beam element corresponding to the virtual displaced configuration and the current configuration is used as the element virtual nodal deformation displacements. The rigid body motion corresponding to the virtual nodal displacements is excluded in the derivation of the element nodal forces. However, in the derivation of the element tangent stiffness matrix, the change of element nodal forces induced by the element rigid body rotation should be considered for the present method. Thus, a stability matrix is included in the element tangent stiffness matrix.

From the numerical examples studied in [36,41], it is found that the convergence rate of solution is slow for some examples with large ratio of the flexural stiffness between the major axis and the minor axis of the cross-section. The present beam element and those beam elements used in [24,36–38,41] are equivalent for rectangular beam with large aspect ratio, because the warping rigidity is negligible. Thus the present beam element and those beam elements used in [24,36–38,41] may have similar convergence rate of solution. Inspection of the element nodal forces and the element stiffness matrices of the present beam element and the beam elements in [24,36–38,41] reveals that the terms relevant to the twist angle, slopes and the length of the beam element will converge to zero and those relevant to the twist rate, curvatures and unit extension will converge to constants. The contribution of the terms relevant to the twist angle, slopes and the length of the beam element may be negligible with the decrease of element size for numerical study. However, their convergence rates may be slower than those relevant to the twist rate, curvatures and unit extension with the decrease of element size. Thus, if the terms relevant to the twist angle, slopes and the length of the beam element are removed from the element nodal forces and the element matrices, the convergence rate of the solution may be increased for numerical studies. This belief will be examined through numerical examples in the paper.

An incremental-iterative method based on the Newton–Raphson method combined with constant arc length of incremental displacement vector is employed for the solution of nonlinear equilibrium equations. The zero value of the tangent stiffness matrix determinant of the structure is used as the criterion of the buckling state, and the corresponding load is the so-called buckling load. Numerical examples are presented to investigate the accuracy and efficiency of the proposed method. The effect of the terms in the element nodal force and tangent stiffness matrix, which will converge to zero with the decrease of element size, on the convergence rate of solution and accuracy for the buckling load and nonlinear behavior of three dimensional beam structures are also investigated through numerical examples.

2. Finite element formulation

2.1. Basic assumptions

The following assumptions are made in the derivation of behavior of the thin-walled beam element with generic open section.

(1) The beam is straight, prismatic and slender, and the Euler–Bernoulli hypothesis is valid.
(2) When the longitudinal normal strain relevant to the twist about the shear center axis is excluded, the unit extension of the centroid axis of the beam element is uniform.
(3) The cross-section of the beam element does not deform in its own plane and strains within this cross-section can be neglected.
(4) The out-of-plane warping of the cross-section is the product of the twist rate of the beam element and the Saint Venant warping function for a prismatic thin walled beam of the same cross-section.
(5) The deformation displacements of the beam element are small.
(6) The material is homogeneous, isotropic and linear elastic.

In this study, Prandtl's membrane analogy and the Saint Venant torsion theory [35,38,45] are used to obtain an approximate Saint Venant warping function for a prismatic thin walled beam.

2.2. Coordinate systems

In this paper, a co-rotational total Lagrangian formulation is adopted. In order to describe the system, we define four sets of right handed rectangular Cartesian coordinate systems:

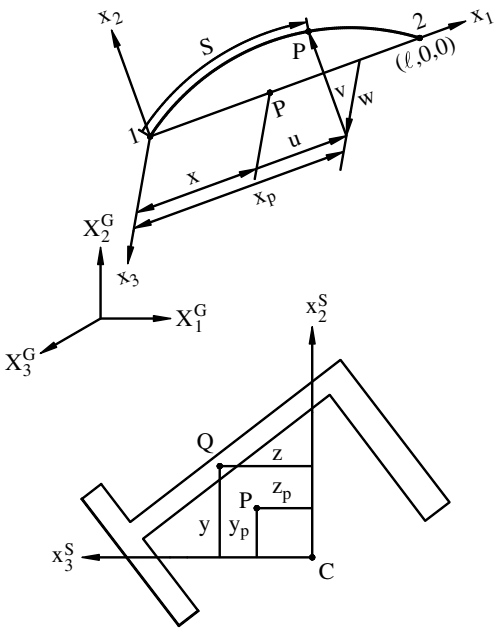

Fig. 1. Coordinate systems.

(1) A fixed global set of coordinates, X_i^G $(i = 1,2,3)$ (see Fig. 1); the nodal coordinates, nodal displacements and rotations, and the stiffness matrix of the system are defined in this coordinates.
(2) Element cross-section coordinates, x_i^S $(i = 1,2,3)$ (see Fig. 1); a set of element cross-section coordinates is associated with each cross-section of the beam element. The origin of this coordinate system is rigidly tied to the *centroid* of the cross section. The x_1^S axis is chosen to coincide with the *normal of the unwarped* cross-section and the x_2^S and x_3^S axes are chosen to be the *principal centroid axes* of the cross-section.
(3) Element coordinates, x_i $(i = 1,2,3)$ (see Fig. 1), a set of element coordinates is associated with each element, which is constructed at the current configuration of the beam element. The origin of this coordinate system is located at node 1, and the x_1 axis is chosen to pass through two end nodes (*shear centers of end sections*) of the element; the directions of the x_2 and x_3 axes are chosen to coincide with the direction of the principal centroidal axes of the cross-section in the undeformed state. The method described in [24] is employed to determine the directions of x_2 and x_3 axes in deformed state. The deformations, internal nodal forces and stiffness matrix of the elements are defined in terms of these coordinates. In this paper, the element deformations are determined by the rotation of element cross section coordinate systems relative to this coordinate system.
(4) Load base coordinates, X_i^P $(i = 1,2,3)$; a set of load base coordinates is associated with each configuration dependent moment. The origin of this coordinate system is chosen to be the node where the configuration dependent moment is applied. The mechanism for generating configuration dependent moment is described in this coordinates, and the corresponding external load and load stiffness matrix are defined in terms of this coordinates.

2.3. Rotation vector

For convenience of the later discussion, the term 'rotation vector' is used to represent a finite rotation. Let $\mathbf{b}$ be a vector, which as a result of the application of a rotation vector $\phi\mathbf{a}$ is transported to the new position $\bar{\mathbf{b}}$. The relation between $\bar{\mathbf{b}}$ and $\mathbf{b}$ may be expressed as [47]

$$\bar{\mathbf{b}} = \cos\phi\mathbf{b} + (1 - \cos\phi)(\mathbf{a}\cdot\mathbf{b})\mathbf{a} + \sin\phi(\mathbf{a}\times\mathbf{b}), \tag{1}$$

where ϕ is the angle of rotation about the axis of rotation, and $\mathbf{a}$ is the unit vector along the axis of rotation.

2.4. Kinematics of beam element

The deformations of the beam element are described in the current element coordinate system. Here, the shear center axis is chosen to be the reference axis and the element nodes are chosen to be located at the shear centers of the end cross-sections of the beam element. Let Q (Fig. 1) be an arbitrary point in the beam element, and P be the point on the shear center axis. The position vector of point Q in the undeformed and deformed configurations may be expressed as

$$\mathbf{r}_0 = x\mathbf{e}_1 + (y - y_p)\mathbf{e}_2 + (z - z_p)\mathbf{e}_3 \tag{2}$$

and

$$\mathbf{r} = x_p(x)\mathbf{e}_1 + v(x)\mathbf{e}_2 + w(x)\mathbf{e}_3 + \theta_{1,x}\omega\mathbf{e}_1^S + (y - y_p)\mathbf{e}_2^S + (z - z_p)\mathbf{e}_3^S, \quad x_p(x) = x + u(x), \tag{3}$$

where y_p and z_p, and y and z are the x_2^S and x_3^S coordinates of point P and Q referred to the element cross-section coordinates, respectively, $u(x)$, $v(x)$, and $w(x)$ are the x_i $(i = 1,2,3)$ components of displacement of point P referred to the current element coordinates, respectively, in the deformed configuration, $\omega = \omega(y,z)$ is the Saint Venant warping function for a prismatic beam of the same cross-section, and $\mathbf{e}_i$

and $\mathbf{e}_i^S$ $(i=1,2,3)$ denote the unit vectors associated with the x_i and x_i^S axes, respectively. Note that the directions of $\mathbf{e}_i$ and $\mathbf{e}_i^S$ are the same in the undeformed state. Here, the orientations of triad $\mathbf{e}_i^S$ in the deformed state is assumed to be determined by the successive application of the following two rotation vectors to the triad $\mathbf{e}_i$

$$\boldsymbol{\theta}_n = \theta_n \mathbf{n}, \quad \boldsymbol{\theta}_t = \theta_1 \mathbf{t}, \tag{4, 5}$$

$$\mathbf{n} = \{0, \theta_2/(\theta_2^2+\theta_3^2)^{1/2}, \theta_3/(\theta_2^2+\theta_3^2)^{1/2}\}, \tag{6}$$

$$\mathbf{t} = \{\cos\theta_n, \theta_3, -\theta_2\}, \tag{7}$$

$$\cos\theta_n = (1-\theta_2^2-\theta_3^2)^{1/2}, \tag{8}$$

$$\theta_2 = -\frac{\mathrm{d}w(x)}{\mathrm{d}s} = -\frac{\mathrm{d}w(x)}{\mathrm{d}x}\frac{\mathrm{d}x}{\mathrm{d}s} = -\frac{w'}{1+\varepsilon_0}, \quad \theta_3 = \frac{\mathrm{d}v(x)}{\mathrm{d}s} = \frac{\mathrm{d}v(x)}{\mathrm{d}x}\frac{\mathrm{d}x}{\mathrm{d}s} = \frac{v'}{1+\varepsilon_0}, \tag{9}$$

$$\varepsilon_0 = \frac{\partial s}{\partial x} - 1 = [(1+u_{,x})^2 + v_{,x}^2 + w_{,x}^2]^{1/2} - 1, \tag{10}$$

where $\mathbf{n}$ is the unit vector perpendicular to the vectors $\mathbf{e}_1$ and $\mathbf{e}_1^S$, and $\mathbf{t}$ is the tangent unit vector of the deformed shear center axis of the beam element. Note that the orientation of $\mathbf{e}_1^S$ coincides with that of $\mathbf{t}$. θ_1 is the rotation about vector $\mathbf{t}$. θ_n is the angle measured from x_1 axis to vector $\mathbf{t}$, ε_0 is the unit extension of the shear center axis and s is the arc length of the deformed shear center axis measured from node 1 to point P. In this paper, θ_i are called rotation parameters, $\boldsymbol{\theta} = \{\theta_1, \theta_2, \theta_3\}$ is the column matrix of rotation parameters, and the symbol $(\,)'$ denotes $(\,)_{,x} = \partial(\,)/\partial x$.

From Eqs. (3) and (10), the relationship among $x_p(x)$, $v(x)$, $w(x)$ in Eq. (3) may be given as

$$x_p(x) = u_1 + \int_0^x [(1+\varepsilon_0)^2 - v_{,x}^2 - w_{,x}^2]^{1/2}\,\mathrm{d}x, \tag{11}$$

where u_1 is the displacement of node 1 in the x_1 direction. Note that due to the definition of the element coordinate system, the value of u_1 is equal to zero. Making use of Eq. (11), one obtains

$$\ell = L + u_2 - u_1 = x_p(L) - x_p(0) = \int_0^L [(1+\varepsilon_0)^2 - v_{,x}^2 - w_{,x}^2]^{1/2}\,\mathrm{d}x, \tag{12}$$

in which ℓ is the current chord length of the shear center axis of the beam element, and L is the length of the undeformed beam axis, and u_2 is the displacement of node 2 in the x_1 direction.

Here, the lateral deflections of the shear center axis, $v(x)$ and $w(x)$, and the rotation about the shear center axis, $\theta_1(x)$, are assumed to be the Hermitian polynomials of x. $v(x)$, $w(x)$ and $\theta_1(x)$ may be expressed by

$$v(x) = \mathbf{N}_b^t \mathbf{u}_b, \quad w(x) = \mathbf{N}_c^t \mathbf{u}_c, \quad \theta_1(x) = \mathbf{N}_d^t \mathbf{u}_d, \tag{13}$$

$$\mathbf{u}_b = \{v_1, v_1', v_2, v_2'\}, \quad \mathbf{u}_c = \{w_1, -w_1', w_2, -w_2'\}, \quad \mathbf{u}_d = \{\theta_{11}, \beta_1, \theta_{12}, \beta_2\}, \tag{14}$$

where v_j and w_j $(j=1,2)$ are nodal values of v and w at nodes j, respectively, v_j' and w_j' $(j=1,2)$ are nodal values of $v_{,x}$ and $w_{,x}$ at nodes j, respectively, and θ_{1j} and β_j $(j=1,2)$ are nodal values of θ_1, $\theta_{1,x}$ at nodes j, respectively. Note that, due to the definition of the element coordinates, the values of v_j and w_j $(j=1,2)$ are zero.

The axial displacements of the shear center axis, $u(x)$ may be determined from the lateral deflections and the unit extension of the shear center axis using Eqs. (3) and (11).

If x, y and z in Eq. (2) are regarded as the Lagrangian coordinates, the Green strain ε_{11}, ε_{12} and ε_{13} are given by [48]

$$\varepsilon_{11} = \tfrac{1}{2}(\mathbf{r}_{,x}^t \mathbf{r}_{,x} - 1), \quad \varepsilon_{12} = \tfrac{1}{2}\mathbf{r}_{,x}^t \mathbf{r}_{,y}, \quad \varepsilon_{13} = \tfrac{1}{2}\mathbf{r}_{,x}^t \mathbf{r}_{,z}. \tag{15a–c}$$

Substituting Eqs. (3) and (11) into Eq. (15a), retaining all terms up to the second order, and excluding the terms relevant to the twist about the shear center axis, ε_c, the corresponding unit extension at the centroid axis of the beam element, may be expressed as [38]

$$\varepsilon_c = \varepsilon_0 + y_p\theta_{3,x} - z_p\theta_{2,x}. \tag{16}$$

Substituting Eq. (16) into Eq. (12) and making use of assumption (2), one may obtain ε_c as

$$\varepsilon_c = \frac{\ell - L}{L} + \frac{y_p}{L}(\theta_{32} - \theta_{31}) - \frac{z_p}{L}(\theta_{22} - \theta_{21}) + \frac{1}{2L}\int_0^L (v_{,x}^2 + w_{,x}^2)\,\mathrm{d}x. \tag{17}$$

Substituting Eqs. (3)–(10) and (16) into Eqs. 15(a)–(c) and retaining all terms up to the second order yields

$$\varepsilon_{11} = \varepsilon_{11}^1 + \varepsilon_{11}^2, \tag{18a}$$

$$\varepsilon_{11}^1 = \varepsilon_c - yv_{,xx} - zw_{,xx} + \omega\theta_{1,xx}, \tag{18b}$$

$$\begin{aligned}\varepsilon_{11}^2 = {} & \tfrac{1}{2}\varepsilon_c^2 + \varepsilon_{0,x}(yv_{,x} + zw_{,x}) + \omega\varepsilon_c\theta_{1,xx} + \tfrac{1}{2}[(y-y_p)^2 + (z-z_p)^2]\theta_{1,x}^2 \\ & + \left(\tfrac{1}{2}y^2 - y_py\right)v_{,xx}^2 + \left(\tfrac{1}{2}z^2 - z_pz\right)w_{,xx}^2 + \tfrac{1}{2}\omega^2\theta_{1,xx}^2 - (y-y_p)\theta_1 w_{,xx} \\ & + (z-z_p)\theta_1 v_{,xx} + (yz - y_pz - z_py)v_{,xx}w_{,xx} - y\omega v_{,xx}\theta_{1,xx} - z\omega w_{,xx}\theta_{1,xx},\end{aligned} \tag{18c}$$

$$\varepsilon_{12} = \varepsilon_{12}^1 + \varepsilon_{12}^2, \tag{19a}$$

$$\varepsilon_{12}^1 = \tfrac{1}{2}[\omega_{,y} - (z-z_p)]\theta_{1,x}, \tag{19b}$$

$$\begin{aligned}\varepsilon_{12}^2 = {} & \tfrac{1}{2}[\omega_{,y}\varepsilon_c\theta_{1,x} + (\omega - y\omega_{,y})\theta_{1,x}v_{,xx} - z\omega_{,y}\theta_{1,x}w_{,xx} + \omega\omega_{,y}\theta_{1,x}\theta_{1,xx}] \\ & + \tfrac{1}{4}(z-z_p)(v_{,x}w_{,xx} - w_{,x}v_{,xx}),\end{aligned} \tag{19c}$$

$$\varepsilon_{13} = \varepsilon_{13}^1 + \varepsilon_{13}^2, \tag{20a}$$

$$\varepsilon_{13}^1 = \tfrac{1}{2}[\omega_{,z} + (y-y_p)]\theta_{1,x}, \tag{20b}$$

$$\begin{aligned}\varepsilon_{13}^2 = {} & \tfrac{1}{2}[\omega_{,z}\varepsilon_c\theta_{1,x} + (\omega - z\omega_{,z})\theta_{1,x}w_{,xx} - y\omega_{,z}\theta_{1,x}v_{,xx} + \omega\omega_{,z}\theta_{1,x}\theta_{1,xx}] \\ & + \tfrac{1}{4}(y-y_p)(w_{,x}v_{,xx} - v_{,x}w_{,xx}),\end{aligned} \tag{20c}$$

where ε_{1j}^k ($j = 1,2,3$; $k = 1,2$) represent the kth order terms of ε_{1j}.

2.5. Nodal parameters and forces

The element proposed here has two nodes with seven degrees of freedom per node. Two sets of element nodal parameters termed 'explicit nodal parameters' and 'implicit nodal parameters' are employed. The explicit nodal parameters of the element are used for the assembly of the system equations from the element equations. They are chosen to be u_{ij} ($u_{1j} = u_j$, $u_{2j} = v_j$, $u_{3j} = w_j$), the x_i ($i = 1,2,3$) components of the translation vectors $\mathbf{u}_j$ at node j ($j = 1,2$), ϕ_{ij}, the x_i ($i = 1,2,3$) components of the rotation vectors $\boldsymbol{\phi}_j$ at node j ($j = 1,2$), and β_j, the twist rate of the shear center axis at node j. Here, the values of $\boldsymbol{\phi}_j$ are reset to zero at current configuration. Thus, $\delta\phi_{ij}$, the variation of ϕ_{ij}, represents infinitesimal rotations about the x_i axes [36], and the generalized nodal forces corresponding to $\delta\phi_{ij}$ are m_{ij}, the conventional moments about the x_i axes. The generalized nodal forces corresponding to δu_{ij}, the variations of u_{ij}, are f_{ij}, the forces in the x_i directions. The generalized nodal forces corresponding to $\delta\beta_j$, the variations of β_j, are bimoment B_j.

Let $\delta\mathbf{u}_j = \{\delta u_j, \delta v_j, \delta w_j\}$, $\delta\boldsymbol{\phi}_j = \{\delta\phi_{1j}, \delta\phi_{2j}, \delta\phi_{3j}\}$, $\delta\beta_j$ ($j = 1,2$) denote the virtual displacement vectors, virtual rotation vectors, and virtual twist rates (referred to as the virtual explicit nodal parameters here) applied at the element nodes j referred to a fixed local element coordinates which are coincident with the

current element coordinates. As a result of the application of the virtual explicit nodal parameters to the current configuration of the beam element, the beam element is displaced to a new configuration. The new configuration is referred to as the virtual displaced configuration in the study. The element coordinates $\bar{x}_i$ $(i=1,2,3)$ and nodal rotation parameters $\bar{\theta}_{ij}$ $(i=1,2,3, j=1,2)$ corresponding to the virtual displaced configuration may be determined by the method described in [24] and the consistent first order linearization. In this paper, a bar over a quantity denotes it is defined in the element coordinates $\bar{x}_i$ $(i=1,2,3)$ corresponding to the virtual displaced configuration.

The relationship between the element coordinates corresponding to the current configuration and the virtual displaced configuration may be expressed by

$$\mathbf{x}=\begin{Bmatrix} x_1 \\ x_2 \\ x_3 \end{Bmatrix}=\begin{bmatrix} 1 & \dfrac{-\Delta v}{\ell} & \dfrac{-\Delta w}{\ell} \\ \dfrac{\Delta v}{\ell} & 1-A_1 & -(\Delta\phi_R+A_2) \\ \dfrac{\Delta w}{\ell} & \Delta\phi_R+A_2 & 1-A_1 \end{bmatrix}\begin{Bmatrix} \bar{x}_1 \\ \bar{x}_2 \\ \bar{x}_3 \end{Bmatrix}=\mathbf{A}_{x\bar{x}}\bar{\mathbf{x}}, \tag{21}$$

where $\Delta v=\delta v_2-\delta v_1$, $\Delta w=\delta w_2-\delta w_1$, $\Delta\phi_R=\frac{1}{2}(\delta\phi_{12}+\delta\phi_{11})$, $A_1=\frac{1}{2}(\theta_{11}\delta\phi_{11}+\theta_{12}\delta\phi_{12})$, $A_2=\frac{1}{4}(\theta_{31}\phi^d_{21}+\theta_{32}\phi^d_{22}-\theta_{21}\phi^d_{31}-\theta_{22}\phi^d_{32})$, $\phi^d_{2j}=\delta\phi_{2j}+\Delta w/\ell$, $\phi^d_{3j}=\delta\phi_{3j}-\Delta v/\ell$. ℓ and θ_{ij} $(i=1,2,3, j=1,2)$ are the chord length and nodal rotation parameters of the beam element at the current configuration, respectively.

If the terms up to the first order of virtual displacements are retained, $\bar{\ell}$ and $\bar{\theta}_{ij}$ $(i=1,2,3, j=1,2)$, the chord length and nodal rotation parameters of the beam element at the virtual displaced configuration, may be expressed by

$$\begin{aligned} &\bar{\ell}=\ell+\Delta u, \\ &\Delta u=\delta u_2-\delta u_1, \end{aligned} \tag{22}$$

$$\begin{aligned} \bar{\theta}_{12}=-\bar{\theta}_{11}=&-\frac{\theta_{11}}{2}+\frac{\theta_{12}}{2}-\frac{\delta\phi_{11}}{2}+\frac{\delta\phi_{12}}{2}-\frac{\Delta v(\theta_{21}-\theta_{22})}{4\ell}-\frac{\Delta w(\theta_{31}-\theta_{32})}{4\ell}-\frac{\theta_{31}\delta\phi_{21}}{4} \\ &+\frac{\theta_{32}\delta\phi_{22}}{4}+\frac{\theta_{21}\delta\phi_{31}}{4}-\frac{\theta_{22}\delta\phi_{32}}{4}, \end{aligned} \tag{23}$$

$$\bar{\theta}_{2j}=\theta_{2j}+\frac{\Delta w}{\ell}+\delta\phi_{2j}-\frac{\Delta v(\theta_{11}+\theta_{12})}{2\ell}+\frac{1}{2}\theta_{3j}\delta\phi_{11}+\frac{1}{2}\theta_{3j}\delta\phi_{12}-\theta_{3j}\delta\phi_{1j}+\frac{\delta\phi_{3j}(\theta_{11}+\theta_{12})}{2},$$

$$\bar{\theta}_{3j}=\theta_{3j}-\frac{\Delta v}{\ell}+\delta\phi_{3j}-\frac{\Delta w(\theta_{11}+\theta_{12})}{2\ell}-\frac{1}{2}\theta_{2j}\delta\phi_{11}-\frac{1}{2}\theta_{2j}\delta\phi_{12}+\theta_{2j}\delta\phi_{1j}-\frac{\delta\phi_{2j}(\theta_{11}+\theta_{12})}{2}.$$

Due to the definition of θ_{1j} $(j=1,2)$, $\theta_{11}+\theta_{12}=0$. However, the variation of $\delta\theta_{11}+\delta\theta_{12}\neq 0$, which should be used in the derivation of the element stiffness matrix and thus retained. The virtual nodal rotation parameters corresponding to the virtual explicit nodal parameters may be given by

$$\delta\bar{\theta}_{ij}=\bar{\theta}_{ij}-\theta_{ij}. \tag{24}$$

The implicit nodal parameters of the element are used to determine the deformation of the beam element. They are chosen to be u_{ij}, the $x_i\,(i=1,2,3)$ components of the translation vectors $\mathbf{u}_j$ at node $j\,(j=1,2)$, θ_{1j}, β_j, $v'_j=(1+\varepsilon_{0j})\theta_{3j}$, and $w'_j=-(1+\varepsilon_{0j})\theta_{3j}$ $(j=1,2)$ defined in Eqs. (9) and (14). Let θ^*_{1j}, θ^*_{2j} and θ_{3j} $(j=1,2)$ denote θ_{1j}, $-w'_j$ and v'_j, respectively. Due to the definition of the element coordinates, the virtual implicit nodal displacements corresponding to the virtual explicit nodal parameters may be given by

$$\delta\bar{u}_1=\delta\bar{v}_1=\delta\bar{v}_2=\delta\bar{w}_1=\delta\bar{w}_2=0, \tag{25}$$

$$\delta\bar{u}_2=\delta\bar{\ell}=\bar{\ell}-\ell=\Delta u, \tag{26}$$

where Δu is defined in Eq. (22).

From Eq. (9), the relation between the virtual implicit nodal parameters $\delta\bar{\theta}^*_{ij}$ $(i=2,3, j=1,2)$ and the virtual nodal rotation parameters $\delta\bar{\theta}_{ij}$ may be given by

$$\delta\bar{\theta}^*_{2j} = -\delta\bar{w}'_j = (1+\varepsilon_{0j})\delta\bar{\theta}_{2j} + \theta_{2j}\delta\varepsilon_{0j}, \tag{27}$$

$$\delta\bar{\theta}^*_{3j} = \delta\bar{v}'_j = (1+\varepsilon_{0j})\delta\bar{\theta}_{3j} + \theta_{3j}\delta\varepsilon_{0j}. \tag{28}$$

From Eqs. (22)–(28), the relations between the variation of the implicit and explicit nodal parameters may be expressed as

$$\delta\bar{\mathbf{q}}_\theta = \mathbf{T}_{\theta\phi}\delta\mathbf{q}, \tag{29}$$

$$\delta\bar{\mathbf{q}}_\theta = \{\delta\bar{\mathbf{u}}_1, \delta\bar{\boldsymbol{\theta}}^*_1, \delta\bar{\mathbf{u}}_2, \delta\bar{\boldsymbol{\theta}}^*_2, \delta\boldsymbol{\beta}\}, \quad \delta\mathbf{q} = \{\delta\mathbf{u}_1, \delta\boldsymbol{\phi}_1, \delta\mathbf{u}_2, \delta\boldsymbol{\phi}_2, \delta\boldsymbol{\beta}\}, \tag{30}$$

where $\delta\bar{\mathbf{u}}_j = \{\delta\bar{u}_j, \delta\bar{v}_j, \delta\bar{w}_j\}$, $\delta\bar{\boldsymbol{\theta}}^*_j = \{\delta\bar{\theta}_{1j}, -\delta\bar{w}'_j, \delta\bar{v}'_j\}$, $(j=1,2)$ and $\delta\boldsymbol{\beta} = \{\delta\beta_1, \delta\beta_2\}$. The explicit form of the matrix $\mathbf{T}_{\theta\phi}$ is given in Appendix A.

The generalized nodal forces corresponding to $\delta\bar{u}_{ij}$, $\delta\bar{\theta}^*_{ij}$ and $\delta\beta_j$ are f^θ_{ij}, m^θ_{ij} and B_j, the generalized forces, the generalized moments, and bimoments, respectively. Note that m^θ_{ij} and f^θ_{ij} are not conventional moments and forces, because $\delta\bar{\theta}^*_{ij}$ are not infinitesimal rotations about the $\bar{x}_i$ axes and $\delta\bar{u}_{ij}$ and $\delta\bar{\theta}^*_{ij}$ are coupled in deformed state.

The global nodal parameters for the structural system corresponding to the element local nodes j $(j=1,2)$ should be consistent with the element explicit nodal parameters. Thus, they are chosen to be U_{ij}, the X_i $(i=1,2,3)$ components of the translation vectors $\mathbf{U}_j$ at node j $(j=1,2)$, Φ_{ij}, the X_i $(i=1,2,3)$ components of the rotation vectors $\boldsymbol{\Phi}_j$ at nodes j $(j=1,2)$, and β_j, the twist rate of the shear center axis at node j. Here, the values of $\boldsymbol{\Phi}_j$ are reset to zero at current configuration. Thus, $\delta\Phi_{ij}$, the variations of Φ_{ij}, represent infinitesimal rotations about the X_i axes [36], and the generalized nodal forces corresponding to $\delta\Phi_{ij}$ are the conventional moments about the X_i axes. The generalized nodal forces corresponding to δU_{ij}, the variation of U_{ij}, are the forces in the X_i directions. The generalized nodal forces corresponding to $\delta\beta_j$, the variation of β_j, are B_j.

2.6. Element nodal force vector

Let $\mathbf{f} = \{\mathbf{f}_1, \mathbf{m}_1, \mathbf{f}_2, \mathbf{m}_2, \mathbf{B}\}$ and $\mathbf{f}_\theta = \{\mathbf{f}^\theta_1, \mathbf{m}^\theta_1, \mathbf{f}^\theta_2, \mathbf{m}^\theta_2, \mathbf{B}\}$ denote the internal nodal force vectors corresponding to the variation of the explicit and implicit nodal parameters, $\delta\mathbf{q}$ and $\delta\bar{\mathbf{q}}_\theta$, respectively, where $\mathbf{f}_j = \{f_{1j}, f_{2j}, f_{3j}\}$, $\mathbf{m}_j = \{m_{1j}, m_{2j}, m_{3j}\}$, $\mathbf{f}^\theta_j = \{f^\theta_{1j}, f^\theta_{2j}, f^\theta_{3j}\}$, $\mathbf{m}^\theta_j = \{m^\theta_{1j}, m^\theta_{2j}, m^\theta_{3j}\}$ $(j=1,2)$, and $\mathbf{B} = \{B_1, B_2\}$.

The element nodal force vector is obtained from the virtual work principle in a fixed local element coordinates which are coincident with the current element coordinates. The virtual work principle requires that

$$\delta W_{\text{ext}} = \delta\mathbf{q}^t\mathbf{f} = \delta W_{\text{int}} = \int_V (\sigma_{11}\delta\bar{\varepsilon}_{11} + 2\sigma_{12}\delta\bar{\varepsilon}_{12} + 2\sigma_{13}\delta\bar{\varepsilon}_{13})\,\mathrm{d}V = \delta\bar{\mathbf{q}}^t_\theta\mathbf{f}_\theta, \tag{31}$$

where V is the volume of the undeformed beam element, $\delta\bar{\varepsilon}_{1j}$ $(j=1,2,3)$ are the variation of ε_{1j} in Eqs. (18)–(20) corresponding to $\delta\bar{\mathbf{q}}_\theta$. σ_{1j} $(j=1,2,3)$ are the second Piola–Kirchhoff stress. For linear elastic material, $\sigma_{11} = E\varepsilon_{11}$, $\sigma_{12} = 2G\varepsilon_{12}$ and $\sigma_{13} = 2G\varepsilon_{13}$, where E is Young's modulus and G is the shear modulus. Note that because $\delta\bar{\varepsilon}_{1j}$ are function of $\delta\bar{\mathbf{q}}_\theta$, δW_{int} may be expressed by $\delta\bar{\mathbf{q}}^t_\theta\mathbf{f}_\theta$. Due to the definition of the element coordinates, the virtual implicit nodal displacements $\delta\bar{u}_1 = \delta\bar{v}_1 = \delta\bar{v}_2 = \delta\bar{w}_1 = \delta\bar{w}_2 = 0$ as mentioned in Eq. (25). The virtual work done by f^θ_{11}, f^θ_{21}, f^θ_{22}, f^θ_{31}, and f^θ_{32} are equal to zero. Thus, f^θ_{11}, f^θ_{21}, f^θ_{22}, f^θ_{31}, and f^θ_{32} have no contribution to explicit nodal force vector $\mathbf{f}$. However, for convenience, they are retained in the derivation of the element internal nodal force.

For convenience, the implicit virtual nodal parameters are divided into four vectors $\delta\bar{\mathbf{u}}_i$ $(i=a,b,c,d)$, where $\delta\bar{\mathbf{u}}_a$ are the variation of $\bar{\mathbf{u}}_a$ given by

$$\bar{\mathbf{u}}_a = \{\bar{u}_1, \bar{u}_2\} \tag{32}$$

and $\delta\bar{\mathbf{u}}_i$ $(i=b,c,d)$ are the variation of $\bar{\mathbf{u}}_i$ defined in Eq. (14).

The generalized force vectors corresponding to $\delta\bar{\mathbf{u}}_i$ $(i = a, b, c, d)$, are

$$\mathbf{f}_a^\theta = \{f_{11}^\theta, f_{12}^\theta\}, \quad \mathbf{f}_b^\theta = \{f_{21}^\theta, m_{31}^\theta, f_{21}^\theta, m_{32}^\theta\},$$
$$\mathbf{f}_c^\theta = \{f_{31}^\theta, m_{21}^\theta, f_{32}^\theta, m_{22}^\theta\}, \quad \mathbf{f}_d^\theta = \{m_{11}^\theta, B_1, m_{12}^\theta, B_2\}. \tag{33}$$

If the element size is chosen to be sufficiently small, the values of the rotation parameters of the deformed element defined in the current element coordinate system may always be much smaller than unity. Thus the higher-order terms of rotation parameters in the element internal nodal forces may be neglected. However, in order to include the nonlinear coupling among the bending, twisting, and stretching deformations, the terms up to the second order of rotation parameters and their spatial derivatives are retained in element internal nodal forces by consistent second-order linearization of Eq. (31). In [37], through numerical study, it was reported that the third order term of the twist rate $\theta_{1,x}$ is the dominant third order term of element nodal forces and should be retained for the geometric nonlinear analysis of doubly symmetric beams with thin-walled open cross-section. It is believed that the behavior of the thin-walled beams with doubly symmetric open cross-section and those with generic open cross-section should be similar. Thus, for simplicity, the third order term of the twist rate $\theta_{1,x}$ is retained in the element nodal forces in this study.

From Eqs. (18)–(20), (31)–(33) and using $\int y\,\mathrm{d}A = \int z\,\mathrm{d}A = \int yz\,\mathrm{d}A = \int \omega\,\mathrm{d}A = \int y\omega\,\mathrm{d}A = \int z\omega\,\mathrm{d}A = 0$, we may obtain

$$\mathbf{f}_a^\theta = [A_1 - AE\varepsilon_c(y_p\mathbf{B}^t\mathbf{u}_b + z_p\mathbf{C}^t\mathbf{u}_c)]\mathbf{G}_a, \tag{34}$$

$$\begin{aligned}
\mathbf{f}_b^\theta = {} & EI_z(1+\varepsilon_c)\int \mathbf{N}_b''v_{,xx}\,\mathrm{d}x + \frac{y_p}{L}A_1\mathbf{B} + \underline{y_pEI_y\int \mathbf{N}_b'''w_{,x}w_{,xx}\,\mathrm{d}x} + \underline{y_pEI_z\int \mathbf{N}_b'''v_{,x}v_{,xx}\,\mathrm{d}x} \\
& + f_{12}^\theta L\mathbf{G}_b - EI_z\int \varepsilon_{0,x}(\underline{\mathbf{N}_b'v_{,xx}} + \underline{\mathbf{N}_b''v_{,x}})\,\mathrm{d}x - \underline{AEz_p\varepsilon_c\int \mathbf{N}_b''\theta_1\,\mathrm{d}x} \\
& + \underline{E(I_z - I_y)\int \mathbf{N}_b''\theta_1 w_{,xx}\,\mathrm{d}x} + \left[GJ_z - \frac{E}{2}(\alpha_z + \alpha_{yz} - 2y_pI_z)\right]\int \mathbf{N}_b''\theta_{1,x}^2\,\mathrm{d}x \\
& - E\left(\frac{3}{2}\alpha_z - 3y_pI_z\right)\int \mathbf{N}_b''v_{,xx}^2\,\mathrm{d}x - E\left(\frac{3}{2}\alpha_{yz} - y_pI_y\right)\int \mathbf{N}_b''w_{,xx}^2\,\mathrm{d}x \\
& - \frac{3}{2}E\alpha_{\omega z}\int \mathbf{N}_b''\theta_{1,xx}^2\,\mathrm{d}x + 3E\alpha_{z\omega}\int \mathbf{N}_b''\theta_{1,xx}v_{,xx}\,\mathrm{d}x + 3E\alpha_{\omega yz}\int \mathbf{N}_b''\theta_{1,xx}w_{,xx}\,\mathrm{d}x \\
& - E(3\alpha_{zy} - 2z_pI_z)\int \mathbf{N}_b''v_{,xx}w_{,xx}\,\mathrm{d}x + \frac{1}{2}GJ\int (\underline{\mathbf{N}_b''\theta_{1,x}w_{,x}} - \underline{\mathbf{N}_b'\theta_{1,x}w_{,xx}})\,\mathrm{d}x,
\end{aligned} \tag{35}$$

$$\begin{aligned}
\mathbf{f}_c^\theta = {} & EI_y(1+\varepsilon_c)\int \mathbf{N}_c''w_{,xx}\,\mathrm{d}x + \frac{z_p}{L}A_1\mathbf{C} + \underline{z_pEI_y\int \mathbf{N}_c'''w_{,x}w_{,xx}\,\mathrm{d}x} + \underline{z_pEI_z\int \mathbf{N}_c'''v_{,x}v_{,xx}\,\mathrm{d}x} \\
& + f_{12}^\theta L\mathbf{G}_c - EI_y\int \varepsilon_{0,x}(\underline{\mathbf{N}_c'w_{,xx}} + \underline{\mathbf{N}_c''w_{,x}})\,\mathrm{d}x + \underline{AEy_p\varepsilon_c\int \mathbf{N}_c''\theta_1\,\mathrm{d}x} \\
& + \underline{E(I_z - I_y)\int \mathbf{N}_c''\theta_1 v_{,xx}\,\mathrm{d}x} - \left[GJ_y + \frac{E}{2}(\alpha_y + \alpha_{zy} - 2z_pI_y)\right]\int \mathbf{N}_c''\theta_{1,x}^2\,\mathrm{d}x \\
& - E\left(\frac{3}{2}\alpha_{zy} - z_pI_z\right)\int \mathbf{N}_c''v_{,xx}^2\,\mathrm{d}x - E\left(\frac{3}{2}\alpha_y - 3z_pI_y\right)\int \mathbf{N}_c''w_{,xx}^2\,\mathrm{d}x \\
& - \frac{3}{2}E\alpha_{\omega y}\int \mathbf{N}_c''\theta_{1,xx}^2\,\mathrm{d}x + 3E\alpha_{\omega yz}\int \mathbf{N}_c''\theta_{1,xx}v_{,xx}\,\mathrm{d}x + 3E\alpha_{y\omega}\int \mathbf{N}_c''\theta_{1,xx}w_{,xx}\,\mathrm{d}x \\
& - E(3\alpha_{yz} - 2y_pI_y)\int \mathbf{N}_c''v_{,xx}w_{,xx}\,\mathrm{d}x + \frac{1}{2}GJ\int (\underline{\mathbf{N}_c'\theta_{1,x}v_{,xx}} - \underline{\mathbf{N}_c''\theta_{1,x}v_{,x}})\,\mathrm{d}x,
\end{aligned} \tag{36}$$

$$\begin{aligned}\mathbf{f}_d^{\theta} = {} & \{GJ + [EI_p + AE(y_p^2 + z_p^2)]\varepsilon_c\} \int \mathbf{N}'_d \theta_{1,x}\,\mathrm{d}x + EI_\omega(1+3\varepsilon_c)\int \mathbf{N}''_d \theta_{1,xx}\,\mathrm{d}x \\ & + \underline{AEy_p\varepsilon_c \int \mathbf{N}_d w_{,xx}\,\mathrm{d}x} - \underline{AEz_p\varepsilon_c \int \mathbf{N}_d v_{,xx}\,\mathrm{d}x} + \left[GJ_\omega + \frac{E}{2}(\alpha_{y\omega} + \alpha_{z\omega})\right]\int \mathbf{N}''_d \theta_{1,x}^2\,\mathrm{d}x \\ & + \frac{3}{2}E\alpha_{y\omega}\int \mathbf{N}''_d w_{,xx}^2\,\mathrm{d}x + \frac{3}{2}E\alpha_{z\omega}\int \mathbf{N}''_d v_{,xx}^2\,\mathrm{d}x + \frac{3}{2}E\alpha_\omega \int \mathbf{N}''_d \theta_{1,xx}^2\,\mathrm{d}x \\ & - 3E\alpha_{\omega y}\int \mathbf{N}''_d \theta_{1,xx} w_{,xx}\,\mathrm{d}x - 3E\alpha_{\omega z}\int \mathbf{N}''_d \theta_{1,xx} v_{,xx}\,\mathrm{d}x + 3E\alpha_{\omega yz}\int \mathbf{N}''_d v_{,xx} w_{,xx}\,\mathrm{d}x \\ & + \underline{E(I_z - I_y)\int \mathbf{N}_d v_{,xx} w_{,xx}\,\mathrm{d}x} + \frac{1}{2}GJ\int \mathbf{N}'_d(\underline{w_{,x} v_{,xx}} - \underline{v_{,x} w_{,xx}})\,\mathrm{d}x \\ & - [2GJ_y + E(\alpha_y + \alpha_{zy} - 2z_p I_y)]\int \mathbf{N}'_d \theta_{1,x} w_{,xx}\,\mathrm{d}x \\ & + [2GJ_z - E(\alpha_z + \alpha_{yz} - 2y_p I_z)]\int \mathbf{N}'_d \theta_{1,x} v_{,xx}\,\mathrm{d}x \\ & + [2GJ_\omega + E(\alpha_{y\omega} + \alpha_{z\omega})]\int \mathbf{N}'_d \theta_{1,x}\theta_{1,xx}\,\mathrm{d}x + \frac{1}{2}EK_I\int \mathbf{N}_d \theta_{1,x}^3\,\mathrm{d}x, \end{aligned} \tag{37}$$

$$\begin{aligned} A_1 = {} & AEL\varepsilon_c + \frac{3}{2}AEL\varepsilon_c^2 + \frac{1}{2}[EI_p + AE(y_p^2 + z_p^2)]\int \theta_{1,x}^2\,\mathrm{d}x + \frac{3}{2}EI_\omega\int \theta_{1,xx}^2\,\mathrm{d}x + \frac{1}{2}EI_y\int w_{,xx}^2\,\mathrm{d}x \\ & + \frac{1}{2}EI_z\int v_{,xx}^2\,\mathrm{d}x + \underline{AEy_p\int \theta_1 w_{,xx}\,\mathrm{d}x} - \underline{AEz_p\int \theta_1 v_{,xx}\,\mathrm{d}x}, \end{aligned} \tag{38}$$

$$\mathbf{B} = \{0,-1,0,1\}, \quad \mathbf{C} = \{0,1,0,-1\}, \quad \mathbf{G}_a = \frac{1}{L}\{-1,1\}, \tag{39}$$

$$\mathbf{G}_b = \underline{\frac{1}{L}\int \mathbf{N}'_b v_{,x}\,\mathrm{d}x} - \frac{y_p}{L}\varepsilon_c\mathbf{B} + \frac{y_p^2}{L^2}\mathbf{Q}_1\mathbf{u}_b + \frac{y_p z_p}{L^2}\mathbf{Q}_2\mathbf{u}_c,$$

$$\mathbf{G}_c = \underline{\frac{1}{L}\int \mathbf{N}'_c w_{,x}\,\mathrm{d}x} - \frac{z_p}{L}\varepsilon_c\mathbf{C} + \frac{y_p z_p}{L^2}\mathbf{Q}_3\mathbf{u}_b + \frac{z_p^2}{L^2}\mathbf{Q}_4\mathbf{u}_c,$$

$$\mathbf{Q}_1 = L(\mathbf{N}'_{b2}\mathbf{N}'''^t_{b2} - \mathbf{N}'_{b1}\mathbf{N}'''^t_{b1} + \mathbf{N}''_{b2}\mathbf{N}''^t_{b2} - \mathbf{N}''_{b1}\mathbf{N}''^t_{b1}) - \mathbf{B}\mathbf{B}^t,$$

$$\mathbf{Q}_2 = \mathbf{Q}_3^t = L(\mathbf{N}'_{b2}\mathbf{N}'''^t_{c2} - \mathbf{N}'_{b1}\mathbf{N}'''^t_{c1} + \mathbf{N}''_{b2}\mathbf{N}''^t_{c2} - \mathbf{N}''_{b1}\mathbf{N}''^t_{c1}) - \mathbf{B}\mathbf{C}^t,$$

$$\mathbf{Q}_4 = L(\mathbf{N}'_{c2}\mathbf{N}'''^t_{c2} - \mathbf{N}'_{c1}\mathbf{N}'''^t_{c1} + \mathbf{N}''_{c2}\mathbf{N}''^t_{c2} - \mathbf{N}''_{c1}\mathbf{N}''^t_{c1}) - \mathbf{C}\mathbf{C}^t,$$

$$\begin{aligned} & I_y = \int z^2\,\mathrm{d}A, \quad I_z = \int y^2\,\mathrm{d}A, \quad K_I = \int [(y-y_p)^2 + (z-z_p)^2]^2\,\mathrm{d}A, \\ & \alpha_y = \int z^3\,\mathrm{d}A, \quad \alpha_z = \int y^3\,\mathrm{d}A, \quad \alpha_{yz} = \int z^2 y\,\mathrm{d}A, \quad \alpha_{zy} = \int y^2 z\,\mathrm{d}A, \\ & I_\omega = \int \omega^2\,\mathrm{d}A, \quad \alpha_\omega = \int \omega^3\,\mathrm{d}A, \quad \alpha_{y\omega} = \int z^2\omega\,\mathrm{d}A, \quad \alpha_{z\omega} = \int y^2\omega\,\mathrm{d}A, \\ & \alpha_{\omega y} = \int \omega^2 z\,\mathrm{d}A, \quad \alpha_{\omega z} = \int \omega^2 y\,\mathrm{d}A, \quad \alpha_{\omega yz} = \int \omega yz\,\mathrm{d}A, \quad I_p = I_y + I_z. \end{aligned} \tag{40}$$

$$J = \int \{[-(z - z_p) + \omega_{,y}]^2 + [(y - y_p) + \omega_{,z}]^2\}\,\mathrm{d}A,$$

$$J_y = \int [(y - y_p)(z\omega_{,z} - \omega) - z(z - z_p)\omega_{,y} + z(\omega_{,y}^2 + \omega_{,z}^2) - \omega\omega_{,z}]\,\mathrm{d}A,$$

$$J_z = \int [(z - z_p)(y\omega_{,y} - \omega) - y(y - y_p)\omega_{,z} - y(\omega_{,y}^2 + \omega_{,z}^2) + \omega\omega_{,y}]\,\mathrm{d}A,$$

$$J_\omega = \int [\omega(\omega_{,y}^2 + \omega_{,z}^2) + (y - y_p)\omega\omega_{,z} - (z - z_p)\omega\omega_{,y}]\,\mathrm{d}A.$$

in which the range of integration for the integral $\int(\,)\,\mathrm{d}x$ in Eqs. (34)–(39) is from 0 to L, A is the cross-section area, $\mathbf{N}_k$ ($k = b, c, d$) are given in Eq. (13), and $\mathbf{N}_{kj}$ are nodal values of $\mathbf{N}_k$ at nodes j ($j = 1, 2$). f_{12}^{θ} in Eqs. (35) and (36) is defined in Eqs. (33) and (34). Eqs. (34)–(39) are calculated using six points Gaussian quadrature and Eq. (40) is calculated analytically in this study.

Note that in Eqs. (34)–(40) the values of L, θ_1, $v_{,x}$ and $w_{,x}$ will converge to zero, and the values of ε_c, $\theta_{1,x}$, $v_{,xx}$ and $w_{,xx}$ will converge to constants with the decrease of the element size. In Eqs. (34)–(39), the underlined terms will converge to zero, and their contribution may be negligible with the decrease of element size for numerical study. However, the convergence rates of L, θ_1, $v_{,x}$ and $w_{,x}$ may be slower than those of ε_c, $\theta_{1,x}$, $v_{,xx}$ and $w_{,xx}$ with the decrease of element size. Thus, if the underlined terms in Eqs. (34)–(39) are removed, the convergence rate of the solution may be increased for numerical studies. This belief will be examined through numerical examples.

From Eqs. (29) and (31), the relation between $\mathbf{f}$ and $\mathbf{f}_\theta$, may be given by

$$\mathbf{f} = \mathbf{T}_{\theta\phi}^{t}\mathbf{f}_\theta, \tag{41}$$

where $\mathbf{T}_{\theta\phi}$ is defined in Eq. (29). Note that only the terms up to the second order of nodal parameters, the third order term of $\theta_{1,x}$, and the third order terms relevant to $f_{12}^{\theta}\mathbf{G}_i L$ ($i = b, c$) are retained in Eq. (41). The explicit form of the relation between $\mathbf{f}$ and $\mathbf{f}_\theta$ is given in Appendix B. In view of Eqs. (B.1), (B.2), (B.6)–(B.9), (35) and (36), one may find that if the terms $f_{12}^{\theta}\mathbf{G}_i L$ ($i = b, c$) in Eqs. (35) and (36) are replaced by $f_{12}\mathbf{G}_i L$, respectively, the terms $f_{12}^{\theta\phi} G_{ij} L$ in Eqs. (B.6)–(B.9) can be eliminated and Eq. (41) can be rewritten by

$$\mathbf{f} = (\mathbf{T}_{\theta\phi}^{0t} + \mathbf{T}_{\theta\phi}^{1t})\mathbf{f}_\theta^{+}, \tag{42}$$

where $\mathbf{T}_{\theta\phi}^{it}$ ($i = 0, 1$) is the ith order terms of $\mathbf{T}_{\theta\phi}$, $\mathbf{f}_\theta^{+}$ is $\mathbf{f}_\theta$ with the terms $f_{12}^{\theta}\mathbf{G}_i L$ ($i = b, c$) in Eqs. (35) and (36) replaced by $f_{12}\mathbf{G}_i L$, respectively. f_{12} is defined in Eq. (B.1).

2.7. Element tangent stiffness matrices

The element tangent stiffness matrix corresponding to the explicit nodal parameters (referred to as explicit tangent stiffness matrix) $\mathbf{k}$ may be defined by

$$\mathrm{d}\mathbf{f} = \mathbf{k}\mathrm{d}\mathbf{q}, \tag{43}$$

where $\mathrm{d}\mathbf{q}$ is a perturbation of the explicit nodal parameter vector and $\mathrm{d}\mathbf{f}$ is the corresponding change of the explicit nodal force vector $\mathbf{f}$. As a result of the application of $\mathrm{d}\mathbf{q}$ to the current configuration of the beam element, the beam element moves to an infinitesimal displaced configuration. Note that $\mathrm{d}\mathbf{q}$ is an actual infinitesimal displacement not a virtual displacement. However, if the quantities $\delta(\,)$ in Eqs. (21)–(24) are replaced by $\mathrm{d}(\,)$, Eq. (21) can be used to express the relationship between the current element coordinates and the infinitesimal displaced element coordinates corresponding to the infinitesimal displaced configuration, and Eqs. (22) and (23) can be used to express the chord length and nodal rotation parameters of the beam element at the infinitesimal displaced configuration. If no confusion may arise, no distinction between $\delta(\,)$ and $\mathrm{d}(\,)$ will be made in this study.

Because $\mathrm{d}\mathbf{q}$ is an actual displacement, the explicit nodal force vector $\mathbf{f}$ translates and rotates with the element from the current element coordinates to the infinitesimal displaced element coordinates. Thus, the change in $\mathbf{f}$ induced by rigid body rotation should be considered.

From Eqs. (21), (29) and (43), $\mathrm{d}\mathbf{f}$ may be expressed by

$$\mathrm{d}\mathbf{f} = \mathrm{d}\mathbf{f}_R + \mathrm{d}\mathbf{f}_d, \tag{44}$$

$$\mathrm{d}\mathbf{f}_R = (\mathbf{T}_R - \mathbf{I}_{14})\mathbf{f} = \mathbf{H}_R \mathrm{d}\mathbf{q}, \tag{45}$$

$$\mathrm{d}\mathbf{f}_d = \frac{\partial \mathbf{f}}{\partial \mathbf{q}}\mathrm{d}\mathbf{q} = \left[\frac{\partial \mathbf{f}}{\partial \bar{\mathbf{q}}_\theta}\frac{\partial \bar{\mathbf{q}}_\theta}{\partial \mathbf{q}}\right]\mathrm{d}\mathbf{q} = \left[\left(\mathbf{T}^{0t}_{\theta\phi}\mathbf{k}_\theta + \mathbf{T}^{1t}_{\theta\phi}\mathbf{k}^0_\theta + \mathbf{H}_\theta\right)\mathbf{T}_{\theta\phi}\right]\mathrm{d}\mathbf{q}, \tag{46}$$

$$\mathbf{T}_R = \begin{bmatrix} \mathbf{A}_{x\bar{x}} & \mathbf{0} & \mathbf{0} & \mathbf{0} & \mathbf{0}_{3\times 2} \\ \mathbf{0} & \mathbf{A}_{x\bar{x}} & \mathbf{0} & \mathbf{0} & \mathbf{0}_{3\times 2} \\ \mathbf{0} & \mathbf{0} & \mathbf{A}_{x\bar{x}} & \mathbf{0} & \mathbf{0}_{3\times 2} \\ \mathbf{0} & \mathbf{0} & \mathbf{0} & \mathbf{A}_{x\bar{x}} & \mathbf{0}_{3\times 2} \\ \mathbf{0}_{2\times 3} & \mathbf{0}_{2\times 3} & \mathbf{0}_{2\times 3} & \mathbf{0}_{2\times 3} & \mathbf{I}_2 \end{bmatrix}, \tag{47}$$

where $\mathrm{d}\mathbf{f}_R$ and $\mathrm{d}\mathbf{f}_d$ are the change in $\mathbf{f}$ induced by rigid body rotation and $\mathrm{d}\bar{\mathbf{q}}_\theta$ corresponding to $\mathrm{d}\mathbf{q}$, respectively. $\mathbf{A}_{x\bar{x}}$ is the transformation matrix between the current element coordinates to the infinitesimal displaced element coordinates, $\mathbf{I}_2$ is the identity matrices of order 2×2, $\mathbf{0}$, $\mathbf{0}_{2\times 3}$ and $\mathbf{0}_{3\times 2}$ are zero matrices of order 3×3, 2×3 and 3×2, respectively. $\mathbf{H}_R$ is a unsymmetrical matrix, which may be called the stability matrix [34]. The explicit form of $\mathbf{H}_R$ is given in Appendix C. $\mathbf{k}_\theta = \partial \mathbf{f}^+_\theta / \partial \bar{\mathbf{q}}_\theta$ is the tangent stiffness matrix corresponding to implicit nodal parameters (referred to as implicit tangent stiffness matrix), $\mathbf{k}^0_\theta$ is the zeroth order terms of nodal parameters of $\mathbf{k}_\theta$, and $\mathbf{H}_\theta = (\partial \mathbf{T}^{1t}_{\theta\phi}/\partial \bar{\mathbf{q}}_\theta)\mathbf{f}^1_\theta$ is an unsymmetrical matrix. The explicit form of the matrix $\mathbf{H}_\theta$ is given in Appendix D.

From Eqs. (43)–(47), the explicit tangent stiffness matrix $\mathbf{k}$ may be expressed by

$$\mathbf{k} = \left[\mathbf{T}^{0t}_{\theta\phi}\mathbf{k}_\theta + \mathbf{T}^{1t}_{\theta\phi}\mathbf{k}^0_\theta + \mathbf{H}_\theta\right]\mathbf{T}_{\theta\phi} + \mathbf{H}_R. \tag{48}$$

Using the direct stiffness method, the implicit tangent stiffness matrix $\mathbf{k}_\theta$ may be assembled by the submatrices

$$\mathbf{k}^\theta_{ij} = \frac{\partial \mathbf{f}^{\theta+}_i}{\partial \bar{\mathbf{u}}_j}, \tag{49}$$

where $\mathbf{f}^{\theta+}_i$ $(i = a, b, c, d)$ are $\mathbf{f}^\theta_i$ defined in Eqs. (34)–(37) with the terms $f^\theta_{12}\mathbf{G}_i L$ $(i = b, c)$ in Eqs. (35) and (36) replaced by $f_{12}\mathbf{G}_i L$, respectively. $\bar{\mathbf{u}}_j$ $(j = a, b, c, d)$ are defined in Eqs. (13) and (32). Note that $\mathbf{k}^\theta_{ij}$ are symmetric matrices. The explicit form of $\mathbf{k}^\theta_{ij}$ may be expressed as

$$\mathbf{k}^\theta_{aa} = AEL\left(1 + 3\varepsilon_c - 2\frac{y_p}{L}\mathbf{B}^t\mathbf{u}_b - 2\frac{z_p}{L}\mathbf{C}^t\mathbf{u}_c\right)\mathbf{G}_a\mathbf{G}^t_a, \tag{50}$$

$$\mathbf{k}^\theta_{ab} = \mathbf{G}_a\left[AEL\mathbf{G}^t_b + AEy_p\left(1 + 2\varepsilon_c - \frac{y_p}{L}\mathbf{B}^t\mathbf{u}_b - \frac{z_p}{L}\mathbf{C}^t\mathbf{u}_c\right)\mathbf{B}^t - \underline{AEz_p\int \mathbf{N}''^t_b\theta_1\,\mathrm{d}x} + EI_z\int \mathbf{N}''^t_b v_{,xx}\,\mathrm{d}x\right],$$

$$\mathbf{k}^\theta_{ac} = \mathbf{G}_a\left[AEL\mathbf{G}^t_c + AEz_p\left(1 + 2\varepsilon_c - \frac{y_p}{L}\mathbf{B}^t\mathbf{u}_b - \frac{z_p}{L}\mathbf{C}^t\mathbf{u}_c\right)\mathbf{C}^t + \underline{AEy_p\int \mathbf{N}''^t_c\theta_1\,\mathrm{d}x} + EI_y\int \mathbf{N}''^t_c w_{,xx}\,\mathrm{d}x\right],$$

$$\mathbf{k}^\theta_{ad} = \mathbf{G}_a\left\{[EI_p + AE(y_p^2 + z_p^2)]\int \mathbf{N}''^t_d\theta_{1,x}\,\mathrm{d}x + AEy_p\int \mathbf{N}^t_d w_{,xx}\,\mathrm{d}x\right.$$
$$\left. - AEz_p\int \mathbf{N}^t_d v_{,xx}\,\mathrm{d}x + 3EI_\omega\int \mathbf{N}''^t_d\theta_{1,xx}\,\mathrm{d}x\right\},$$

$$\mathbf{k}^{\theta}_{bb} = EI_z(1+\varepsilon_c)\int \mathbf{N}''_b\mathbf{N}'''^{t}_b\,\mathrm{d}x + \frac{AEy_p^2}{L}[(1+2\varepsilon_c)\mathbf{B}\mathbf{B}^t + \varepsilon_c\mathbf{Q}_1]$$
$$+ AEy_p(\mathbf{G}_b\mathbf{B}^t + \mathbf{B}\mathbf{G}^t_b) - \underline{\frac{AEy_pz_p}{L}\int (\mathbf{N}''_b\mathbf{B}^t + \mathbf{B}\mathbf{N}'''^{t}_b)\theta_1\,\mathrm{d}x}$$
$$- EI_z\varepsilon_{0,x}\int (\mathbf{N}'_b\mathbf{N}'''^{t}_b + \mathbf{N}''_b\mathbf{N}''^{t}_b)\,\mathrm{d}x + f_{12}\int \mathbf{N}'_b\mathbf{N}''^{t}_b\,\mathrm{d}x + 3E\alpha_{z\omega}\int \mathbf{N}''_b\mathbf{N}'''^{t}_b\theta_{1,xx}\,\mathrm{d}x$$
$$- 3E(\alpha_z - 2y_pI_z)\int \mathbf{N}''_b\mathbf{N}'''^{t}_b v_{,xx}\,\mathrm{d}x - E(3\alpha_{zy} - 2z_pI_z)\int \mathbf{N}''_b\mathbf{N}'''^{t}_b w_{,xx}\,\mathrm{d}x$$
$$+ y_pEI_z\int\left[\left(\mathbf{N}'''_b\mathbf{N}'^{t}_b + \mathbf{N}'_b\mathbf{N}''''^{t}_b + \frac{1}{L}\mathbf{N}''_b\mathbf{B}^t + \frac{1}{L}\mathbf{B}\mathbf{N}'''^{t}_b\right)v_{,xx} + \underline{(\mathbf{N}'''_b\mathbf{N}'''^{t}_b + \mathbf{N}''_b\mathbf{N}''''^{t}_b)v_{,x}}\right]\mathrm{d}x,$$

$$\mathbf{k}^{\theta}_{bc} = AEy_p\mathbf{B}\mathbf{G}^t_c + AEz_p\mathbf{G}_b\mathbf{C}^t + \underline{\frac{AEy_p^2}{L}\int \mathbf{B}\mathbf{N}'''^{t}_c\theta_1\,\mathrm{d}x} - \underline{\frac{AEz_p^2}{L}\int \mathbf{N}''_b\mathbf{C}^t\theta_1\,\mathrm{d}x}$$
$$+ \frac{AEy_pz_p}{L}[(1+2\varepsilon_c)\mathbf{B}\mathbf{C}^t + \varepsilon_c\mathbf{Q}_2] + \underline{E(I_z - I_y)\int \mathbf{N}''_b\mathbf{N}'''^{t}_c\theta_1\,\mathrm{d}x}$$
$$+ y_pEI_y\int\left[\left(\mathbf{N}'''_b\mathbf{N}'^{t}_c + \frac{1}{L}\mathbf{B}\mathbf{N}'''^{t}_c\right)w_{,xx} + \underline{\mathbf{N}'''_b\mathbf{N}'''^{t}_c w_{,x}}\right]\mathrm{d}x$$
$$+ z_pEI_z\int\left[\left(\mathbf{N}'_b\mathbf{N}''''^{t}_c + \frac{1}{L}\mathbf{N}''_b\mathbf{C}^t\right)v_{,xx} + \underline{\mathbf{N}''_b\mathbf{N}''''^{t}_c v_{,x}}\right]\mathrm{d}x$$
$$+ 3E\alpha_{\omega yz}\int \mathbf{N}''_b\mathbf{N}'''^{t}_c\theta_{1,xx}\,\mathrm{d}x - E(3\alpha_{zy} - 2z_pI_z)\int \mathbf{N}''_b\mathbf{N}'''^{t}_c v_{,xx}\,\mathrm{d}x$$
$$- E(3\alpha_{yz} - 2y_pI_y)\int \mathbf{N}''_b\mathbf{N}'''^{t}_c w_{,xx}\,\mathrm{d}x + \frac{1}{2}GJ\int (\mathbf{N}''_b\mathbf{N}'^{t}_c - \mathbf{N}'_b\mathbf{N}'''^{t}_c)\theta_{1,x}\,\mathrm{d}x,$$

$$\mathbf{k}^{\theta}_{bd} = \frac{y_p}{L}[EI_p + AE(y_p^2 + z_p^2)]\int \mathbf{B}\mathbf{N}'^{t}_d\theta_{1,x}\,\mathrm{d}x - AEz_p\varepsilon_c\int \mathbf{N}''_b\mathbf{N}^t_d\,\mathrm{d}x$$
$$+ \frac{3y_pEI_\omega}{L}\int \mathbf{B}\mathbf{N}'''^{t}_d\theta_{1,xx}\,\mathrm{d}x + \frac{AEy_p^2}{L}\int \mathbf{B}\mathbf{N}^t_d w_{,xx}\,\mathrm{d}x - \frac{AEy_pz_p}{L}\int \mathbf{B}\mathbf{N}^t_d v_{,xx}\,\mathrm{d}x$$
$$- 3E\alpha_{\omega z}\int \mathbf{N}''_b\mathbf{N}'''^{t}_d\theta_{1,xx}\,\mathrm{d}x + 3E\alpha_{z\omega}\int \mathbf{N}''_b\mathbf{N}'''^{t}_d v_{,xx}\,\mathrm{d}x + 3E\alpha_{\omega yz}\int \mathbf{N}''_b\mathbf{N}'''^{t}_d w_{,xx}\,\mathrm{d}x$$
$$+ E(I_z - I_y)\int \mathbf{N}''_b\mathbf{N}^t_d w_{,xx}\,\mathrm{d}x + \frac{1}{2}GJ\int \underline{(\mathbf{N}''_b\mathbf{N}'^{t}_d w_{,x}} - \mathbf{N}'_b\mathbf{N}'^{t}_d w_{,xx})\,\mathrm{d}x$$
$$+ [2GJ_z - E(\alpha_z + \alpha_{yz} - 2y_pI_z)]\int \mathbf{N}''_b\mathbf{N}'^{t}_d\theta_{1,x}\,\mathrm{d}x,$$

$$\mathbf{k}^{\theta}_{cc} = EI_y(1+\varepsilon_c)\int \mathbf{N}''_c\mathbf{N}'''^{t}_c\,\mathrm{d}x + \frac{AEz_p^2}{L}[(1+2\varepsilon_c)\mathbf{C}\mathbf{C}^t + \varepsilon_c\mathbf{Q}_4]$$
$$+ AEz_p(\mathbf{G}_c\mathbf{C}^t + \mathbf{C}\mathbf{G}^t_c) + \underline{\frac{AEy_pz_p}{L}\int (\mathbf{N}''_c\mathbf{C}^t + \mathbf{C}\mathbf{N}'''^{t}_c)\theta_1\,\mathrm{d}x}$$
$$- EI_y\varepsilon_{0,x}\int (\mathbf{N}'_c\mathbf{N}'''^{t}_c + \mathbf{N}''_c\mathbf{N}''^{t}_c)\,\mathrm{d}x + f_{12}\int \mathbf{N}'_c\mathbf{N}''^{t}_c\,\mathrm{d}x + 3E\alpha_{y\omega}\int \mathbf{N}''_c\mathbf{N}'''^{t}_c\theta_{1,xx}\,\mathrm{d}x$$
$$- E(3\alpha_{yz} - 2y_pI_y)\int \mathbf{N}''_c\mathbf{N}'''^{t}_c v_{,xx}\,\mathrm{d}x - 3E(\alpha_y - 2z_pI_y)\int \mathbf{N}''_c\mathbf{N}'''^{t}_c w_{,xx}\,\mathrm{d}x$$
$$+ z_pEI_y\int\left[\left(\mathbf{N}'''_c\mathbf{N}'^{t}_c + \mathbf{N}'_c\mathbf{N}''''^{t}_c + \frac{1}{L}\mathbf{N}''_c\mathbf{C}^t + \frac{1}{L}\mathbf{C}\mathbf{N}''^{\mathbf{t}}_c\right)w_{,xx} + \underline{(\mathbf{N}'''_c\mathbf{N}''^{t}_c + \mathbf{N}''_c\mathbf{N}''''^{t}_c)w_{,x}}\right]\mathrm{d}x,$$

$$\mathbf{k}^{\theta}_{cd} = \frac{z_p}{L}[EI_p + AE(y_p^2 + z_p^2)] \int \mathbf{C}\mathbf{N}''^{t}_{d}\theta_{1,x}\,\mathrm{d}x + AEy_p\varepsilon_c \int \mathbf{N}''_c\mathbf{N}'^{t}_{d}\,\mathrm{d}x$$
$$+ \frac{3z_pEI_\omega}{L} \int \mathbf{C}\mathbf{N}'''^{t}_{d}\theta_{1,xx}\,\mathrm{d}x - \frac{AEz_p^2}{L} \int \mathbf{C}\mathbf{N}'^{t}_{d}v_{,xx}\,\mathrm{d}x + \frac{AEy_pz_p}{L} \int \mathbf{C}\mathbf{N}^{t}_{d}w_{,xx}\,\mathrm{d}x$$
$$- 3E\alpha_{\omega y} \int \mathbf{N}''_c\mathbf{N}'''^{t}_{d}\theta_{1,xx}\,\mathrm{d}x + 3E\alpha_{\omega yz} \int \mathbf{N}''_c\mathbf{N}'''^{t}_{d}v_{,xx}\,\mathrm{d}x + 3E\alpha_{y\omega} \int \mathbf{N}''_c\mathbf{N}'''^{t}_{d}w_{,xx}\,\mathrm{d}x$$
$$+ E(I_z - I_y) \int \mathbf{N}''_c\mathbf{N}'^{t}_{d}v_{,xx}\,\mathrm{d}x + \frac{1}{2}GJ \int (\mathbf{N}'_c\mathbf{N}''^{t}_{d}v_{,xx} - \underline{\mathbf{N}''_c\mathbf{N}''^{t}_{d}v_{,x}})\,\mathrm{d}x$$
$$- [2GJ_y + E(\alpha_y + \alpha_{zy} - 2z_pI_y)] \int \mathbf{N}''_c\mathbf{N}''^{t}_{d}\theta_{1,x}\,\mathrm{d}x,$$

$$\mathbf{k}^{\theta}_{dd} = \{GJ + [EI_p + AE(y_p^2 + z_p^2)]\varepsilon_c\} \int \mathbf{N}'_d\mathbf{N}''^{t}_{d}\,\mathrm{d}x + EI_\omega(1 + 3\varepsilon_c) \int \mathbf{N}''_d\mathbf{N}'''^{t}_{d}\,\mathrm{d}x$$
$$+ 3E\alpha_\omega \int \mathbf{N}''_d\mathbf{N}'''^{t}_{d}\theta_{1,xx}\,\mathrm{d}x - 3E\alpha_{\omega y} \int \mathbf{N}''_d\mathbf{N}'''^{t}_{d}w_{,xx}\,\mathrm{d}x - 3E\alpha_{\omega z} \int \mathbf{N}''_d\mathbf{N}'''^{t}_{d}v_{,xx}\,\mathrm{d}x$$
$$- [2GJ_y + E(\alpha_y + \alpha_{zy} - 2z_pI_y)] \int \mathbf{N}'_d\mathbf{N}''^{t}_{d}w_{,xx}\,\mathrm{d}x$$
$$+ [2GJ_z - E(\alpha_z + \alpha_{yz} - 2y_pI_z)] \int \mathbf{N}'_d\mathbf{N}''^{t}_{d}v_{,xx}\,\mathrm{d}x$$
$$+ [2GJ_\omega + E(\alpha_{y\omega} + \alpha_{z\omega})] \int [\mathbf{N}'_d\mathbf{N}''^{t}_{d}\theta_{1,xx} + (\mathbf{N}'_d\mathbf{N}'''^{t}_{d} + \mathbf{N}''_d\mathbf{N}''^{t}_{d})\theta_{1,x}]\,\mathrm{d}x$$
$$+ \frac{3}{2}EK_I \int \mathbf{N}'_d\mathbf{N}''^{t}_{d}\theta_{1,x}^2\,\mathrm{d}x,$$

where the underlined terms will converge to zero with the decrease of element size and may be removed for numerical study based on the same reason mentioned in last section for element nodal forces.

The element tangent stiffness matrix referred to the global coordinate system is obtained by using the standard coordinate transformation.

2.8. Load stiffness matrix

Different ways for generating configuration dependent moment were proposed in the literature [9,11,33]. Here, only the conservative moments generated by conservative force or forces (with fixed directions) are considered, and the ways for generating conservative moment proposed in [33] are employed here. In this study, a set of load base coordinates X_i^P $(i = 1, 2, 3)$ associated with each configuration dependent moment are constructed at the current configuration. The mechanism for generating configuration dependent moment is described in this coordinates, and the corresponding external load and load stiffness matrix [49] are defined in terms of this coordinates. However, the description of the ways for generating conservative moment and the corresponding load stiffness matrices are not repeated here.

2.9. Equilibrium equations

The nonlinear equilibrium equations may be expressed by

$$\mathbf{\Psi} = \mathbf{F} - \lambda\mathbf{P} = \mathbf{0}, \tag{51}$$

where $\mathbf{\Psi}$ is the unbalanced force between the internal nodal force $\mathbf{F}$ and the external nodal force $\lambda\mathbf{P}$, where λ is the loading parameter, and $\mathbf{P}$ is a reference loading. Note that $\mathbf{P}$ may require to be updated at each iter-

ation, if the applied load is configuration dependent. **F** is assembled from the element nodal force vectors, which are calculated using Eqs. (34)–(37) and (42) first in a fixed local element coordinates which are coincident with the current element coordinates and then transformed from the local element coordinate system to global coordinate system before assemblage using standard procedure. Note that the element global translation vectors $\mathbf{U}_j$ at node j ($j = 1, 2$) are only used to determine the current element nodal coordinates in this study and the rigid body motions of the beam element are removed using the method proposed in [24]. Thus, the projector matrix [50,51], which relates the variations of the local displacements to the variations of the global ones, may not be required here.

In this paper, an weighted Euclidean norm of the unbalanced force is employed as the error measure for the equilibrium iterations, and is given by

$$\frac{\|\mathbf{\Psi}\|}{|\lambda|\sqrt{N}} \leqslant e_{\text{tol}}, \tag{52}$$

where N is the number of equilibrium equations; e_{tol} is a prescribed value of error tolerance. Unless otherwise stated, the error tolerance e_{tol} is set to 10^{-6} in this study.

2.10. Criterion of the buckling state

Let $\mathbf{K}_T(\lambda)$ denote the tangent stiffness matrix of the structure corresponding to the loading parameter λ. The criterion of the buckling state used here may be expressed as

$$D(\lambda) = \det|\mathbf{K}_T(\lambda)| = 0. \tag{53}$$

Here, the buckling loading parameter λ_{NB} denotes the minimum loading parameter satisfying Eq. (52).

3. Numerical algorithm

An incremental-iterative method based on the Newton–Raphson method combined with constant arc length of incremental displacement vector [52] is employed for the solution of nonlinear equilibrium equations. The Euler predictor is used for the initial displacement increment. For a given displacement increment or corrector, the method described in [24,53] is employed to determine the current element cross-section coordinates, element coordinates and element deformation nodal parameters for each element. The parabolic interpolation method of the arc length proposed in [37] is employed here to find the buckling load. In order to initiate the secondary path, at the bifurcation point a perturbation displacement proportional to the corresponding buckling mode is added [54].

4. Numerical studies

In order to investigate the effect of the underlined terms in Eqs. (34)–(39), (50), (A.3) and (B.5)–(B.9) on the convergence rate of solution and accuracy for the buckling load and nonlinear behavior of three dimensional beam structures, the following cases are considered:

1. EA—All terms in Eqs. (34)–(39), (50), (A.3) and (B.5)–(B.9) are considered.
2. EB—All underlined terms in Eqs. (34)–(39), (50), (A.3) and (B.5)–(B.9) are dropped.

For convenience, the elements used for cases EA and EB are called EA element and EB element, respectively. Let α denote the ratio of the flexural stiffness between the major axis and the minor axis of the cross-section of the beam.

Example 1 (*Buckling of a cantilever beam subjected to end torque*). The example considered here is a cantilever beam of rectangular section subjected to end torque T as shown in Fig. 2. This example was first studied by Hsiao and Lin [36]. However, the warping rigidity is not considered in [36]. The ends of the beam are warping free. The geometry and material properties are given in Fig. 2. The configuration dependent torque is generated by the strings wound around a great circle of a sphere rigidly connected with at node A and acted upon by forces [33] as shown in Fig. 2. The magnitude of the end torque $T = 2PR$, where R is the radius of great circle of the sphere. The present buckling moments T_{NB} and their relative error with respect to the buckling moment obtained using 160 EB elements are shown in Table 1. It can be seen that the buckling moments may converge to the same value for cases EA and EB. However, convergence rate for case EB is much faster than that for case EA. In [36], the buckling moment T_{NB} (10^3 kN cm) obtained using 200 elements are 3.532, 1.497, and 3.177 for QT1, QT2, and ST moments, respectively. The agreement between the present buckling moments and those given in [36] is very good. Because the EA element and the element used in [36] are equivalent for this example, the convergence rate of buckling moment given in [36] is similar to that for EA element. Note that for this example, the only nonzero displacements are the translation along and rotation about the beam axis. Consequently, $E(I_z - I_y)\int \mathbf{N}_b''\mathbf{N}_c'''\theta_1\,dx$ in $\mathbf{k}_{bc}^{\theta}$(in Eq. (50)) is the only nontrivial underlined term in Eqs. (34)–(39), (50), (A.3) and (B.5)–(B.9). If $I_y = I_z(\alpha = 1)$, the EA and EB elements are identical. However, for this example, the value of α is 400. Thus, the slow convergence rate for the EA element may be attributed to the large ratio of the flexural stiffness between the major axis and the minor axis of the cross-section. The element used in [36] with the term $E(I_z - I_y)\int \mathbf{N}_b''\mathbf{N}_c'''\theta_1\,dx$ dropped is also tested. As expected, the convergence rate of buckling moment is similar to that for EB element.

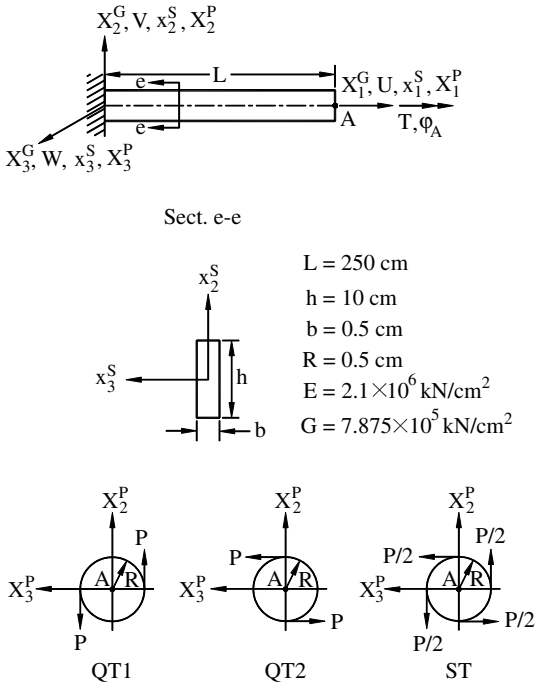

Fig. 2. Cantilever beam of rectangular section subjected to end torque (Example 1).

Table 1
Buckling load for Example 1

Moment type	Element no.	Buckling moment T_{NB} (10^3 kNcm)			
		EA	Error (%)	EB	Error (%)
QT1	2	0.45883	−87.0363	3.90562	10.3471
	4	0.91974	−74.0141	3.62605	2.44822
	10	2.53611	−28.3462	3.55301	0.38480
	20	3.14053	−11.2693	3.54275	0.09487
	40	3.42616	−3.19922	3.54019	0.02260
	60	3.48759	−1.46355	3.53972	0.00922
	80	3.50993	−0.83248	3.53956	0.00454
	160	3.53191	−0.21140	3.53939	0.00000
QT2	2	0.43083	−71.2570	1.56021	4.08984
	4	0.75576	−49.5795	1.51359	0.97963
	10	1.21125	−19.1914	1.50123	0.15441
	20	1.40261	−6.42479	1.49948	0.03805
	40	1.47231	−1.77475	1.49905	0.00902
	60	1.48684	−0.80535	1.49897	0.00365
	80	1.49207	−0.45661	1.49894	0.00177
	160	1.49718	−0.11537	1.49891	0.00000
ST	2	0.44970	−85.9076	3.96922	24.3853
	4	0.86563	−72.8735	3.34234	4.74058
	10	1.78568	−44.0414	3.21387	0.71440
	20	2.51751	−21.1075	3.19666	0.17512
	40	2.95902	−7.27186	3.19240	0.04160
	60	3.07919	−3.50585	3.19161	0.01693
	80	3.12612	−2.03528	3.19133	0.00830
	160	3.17425	−0.52710	3.19107	0.00000

Example 2 (*Deployable ring subjected to a fixed axis moment*). The example considered is ring subjected to a fixed axis moment M at point A as shown in Fig. 3. The ring is clamped at point O. Point A is restricted to translate along and rotate about the X_1^G axis only. The geometry and material properties are given in Fig. 3. This example was introduced by Goto et al. [55] and studied by Battini and Pacoste [40] also.

The error tolerance $e_{\text{tol}} = 10^{-7}$ is used for this example. The load–deflection curves of the present study together with the results given in [40] are shown in Fig. 4. It can be seen that the agreement between the present results obtained using 60 EB elements and the results obtained using 128 t3dl elements [40] is very good. The results of 60 EB elements are obtained by using 67 increments. The average number of iterations per increment is about 16. The results of 60 EB elements are nearly identical to the results of 120 EB elements (not shown here). The results of 180 EA elements are also shown in Fig. 4. It can be seen that the convergence rate of the EB element is about three times as fast as that of the EA element. For this example, the value of α is 100. Thus, the slow convergence rate for the EA element may be attributed to the large ratio of the flexural stiffness between the major axis and the minor axis of the cross-section as Example 1.

Example 3 (*Simply supported right-angle frame subjected to uniform moment*). The example considered is a simply supported angle frame subjected to uniform moment as shown in Fig. 5. The ends of the beam are free to warp and free to rotate about X_3^G axis, but restrained from rotation about X_1^G and X_2^G axes. The translation is restrained at end point A, and is free only in the direction of X_1^G axis at points B. Due to

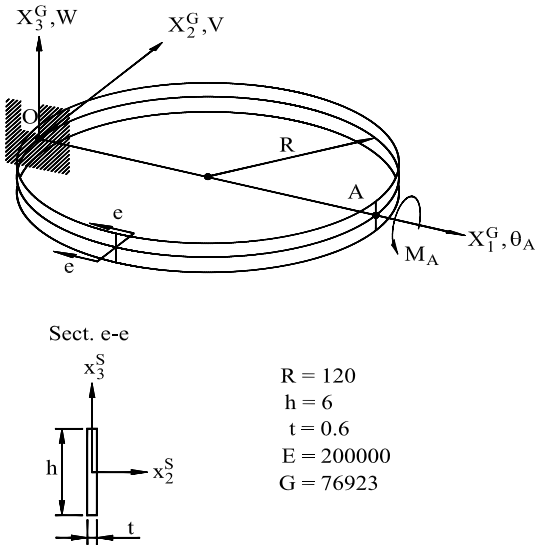

Fig. 3. Deployable ring subjected to a fixed axis moment (Example 2).

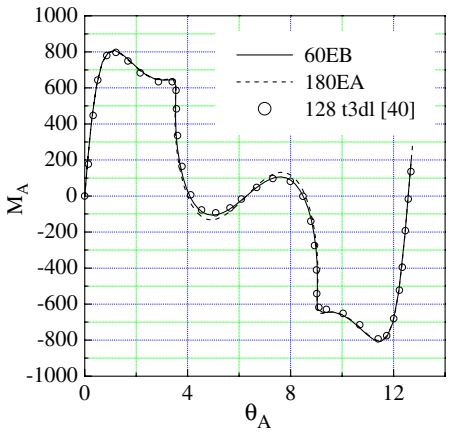

Fig. 4. Load–twist angle curves for Example 2.

symmetry, only half of the frame is analyzed. The nontrivial cross-section constants are: $I_y = 0.54$ mm^4, $I_z = 1350$ mm^4, $J = 2.133$ mm^4, $I_\omega = 40.43$ mm^6, $K_I = 1.823 \times 10^5$ mm^6, $\alpha_{\omega yz} = 40.462$ mm^6. The theoretical linear buckling moment is $M_{cr} = (\pi/L)\sqrt{EI_yGJ} = 618.31$ N mm [4]. The present buckling moment obtained using 10, 20 EB and 40 EA elements are $M_{NB} = 620.78$, 620.77, and 620.77 N mm^{-1}, respectively.

The results of 10 EB elements and 20 EB elements are obtained by using 68 and 56 increments, respectively. The average numbers of iterations per increment are about 14 and 13, respectively. The load–deflection curves of the present study are shown in Fig. 6. The results of [40] obtained using 10 t3d and tw3d elements are also shown in Fig. 6. It can be seen that the agreement between the results of 10 EB elements and the results of [40] is very good. It is reported that a stable bifurcation point is reached at a slightly higher value of the buckling moment in [40]. A stable bifurcation point is observed at about $M =$

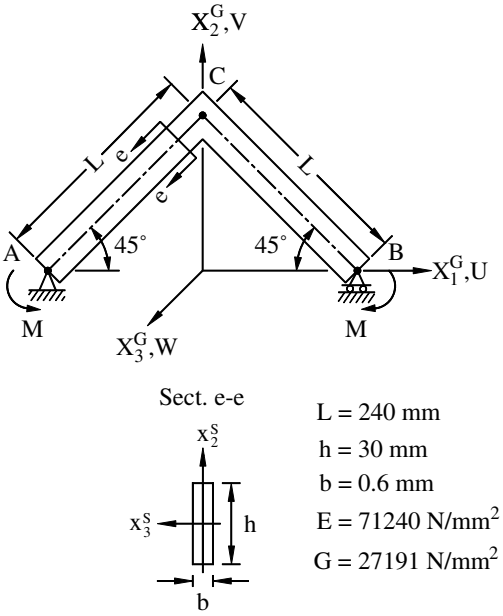

Fig. 5. Simply supported right-angle frame subjected to uniform moment (Example 3).

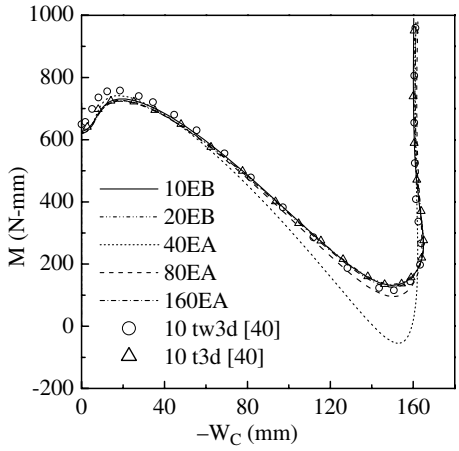

Fig. 6. Load–displacement (W_C) curves for Example 3.

628 N mm^{-1} for the results of 10 EB elements. This result is consistent with that reported in [40]. However, the bifurcation point is reached at the value of buckling moment for the rest results of the present study shown in Fig. 6. Similar to the results of [36,40], a limit point is reached at the moment of about $1.2M_{NB}$ for the secondary path. The discrepancy among the results of 40 EA, 80 EA and 10 EB elements is remarked when the displacements are large. The agreement among the results of 160 EA elements, 10 EB elements and 20 EB elements is very good. The value of α is 2500 for this example. This may explain why the

convergence rate of the EB element is much faster than that of the EA element for this example. The curves of load verse components of the internal moment at node C are shown in Fig. 7. In Fig. 7, M_i^G $(i = 1,2,3)$ denote the X_i^G components of the internal moment referred to the global coordinates, and M_i $(i = 1,2,3)$ denote the x_i components of the internal moment referred to the current element coordinates. As expected, the magnitude of M_3^G is equal to that of the applied moment and M_1^G is equal zero.

Example 4 (*Simply supported beam of angle section subjected to a mid-span torque and constant end moments*). The example considered is a simply supported beam of monosymmetric angle cross-section subjected to a mid-span torque T and equal constant end moments M applied about its symmetric axis as shown in Fig. 8. This example was experimentally and theoretically studied by Engel and Goodier [1].

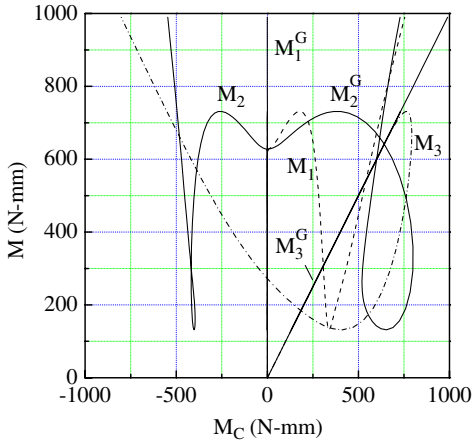

Fig. 7. Load–internal nodal moments (node C) curves for Example 3.

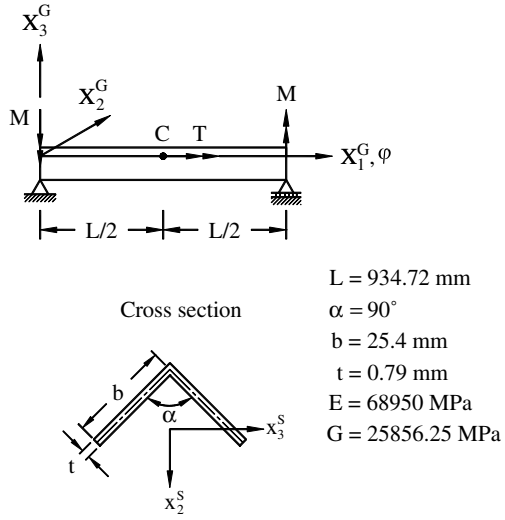

Fig. 8. Simply supported beam of angle section subjected to a mid-span torque and constant end moments (Example 4).

The ends of the beam are free to warp and free to rotate about X_2^G and X_3^G axes, but restrained from rotation about X_1^G axis. The translation is restrained at left end point, and is free only in the direction of X_1^G axis at right end point. The geometry and material (61 S-T aluminum) properties are shown in Fig. 8. The self-weight of the beam is 1.00258 N. For investigating the influence of the bending moments on the torsional rigidity, seven different values of M are considered: M (N m) = 0, 2.44, 4.89, 7.34, 8.56, 9.78, and 11.0 (transcribed by the authors).

The present results are obtained using 10 EB elements and 10 EA elements. The load–deflection curves of the present study together with the experimental results given in [1] are shown in Fig. 9, where the initial deflections caused by the self-weight are excluded. It can be seen that the agreement between these two results is very good. Note that the value of α is about 4 for this example. This may explain why the difference between the convergence rate of the EA and EB element is insignificant for this example.

Example 5 (*Torsional buckling for beam of cruciform cross-section subjected to an axial force*). This example considered is the beam of cruciform cross-section subjected to an axial force P as shown in Fig. 10. This example was introduced by Battini and Pacoste [40]. Except the translation is free in the direction of X_1^G axis at the right end, the translations, rotations and warping are restrained at both ends of the beam. Note that for this example, the only nonzero displacements are the translation along and rotation about the beam axis, and $I_y = I_z$. Thus, the EA and EB elements are identical for this example. In [40], the term $\frac{1}{2}u_{1,1}^2$ in ε_{11} is neglected. In order to compare results with those given in [40], the EB element with the terms $\frac{3}{2}AEL\varepsilon_c^2$ in A_1 (Eq. (38)) and $3EI_\omega\varepsilon_c \int \mathbf{N}_d''\mathbf{N}_d'''^t \,\mathrm{d}x$ in $\mathbf{k}_{dd}^\theta$ (Eq. (50)) neglected, referred to as EC element, are also considered for this example.

The present buckling loads obtained using 10 elements together with those given in [18,40] are shown in Table 2. It can be seen that the agreement among these results is very good. The results obtained using EB and EC elements are a little bit different, which shows that the term $\frac{1}{2}u_{1,1}^2$ in ε_{11} has some minor effect on the buckling load for this example. The load–deflection curves of the present study for postbuckling analysis together with the results of [40] are shown in Fig. 11. It can be seen that the discrepancy between the deflection curves obtained using 10 and 20 EB elements is increased with the increase of the twist angle. The

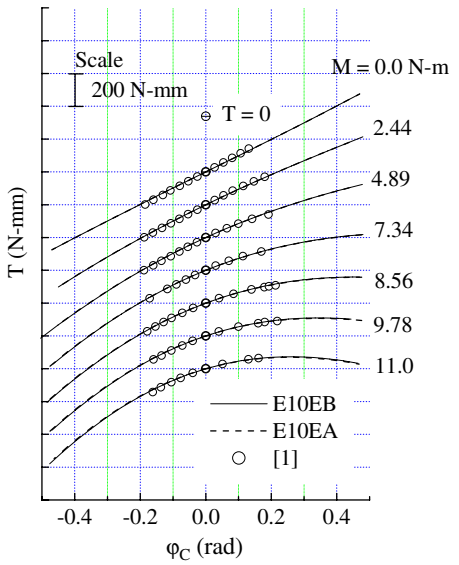

Fig. 9. Load–twist angle curves for Example 4.

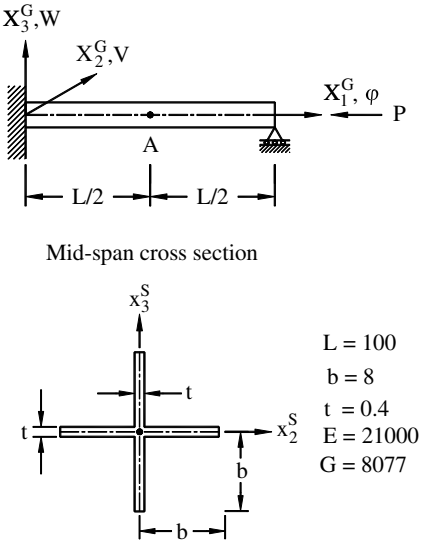

Fig. 10. Beam of cruciform cross-section subjected to an axial force (Example 5).

Table 2
Torsional buckling load for Example 5

Mode no.	Buckling load, P_{NB}			
	Theory [18]	10 bw3d [40]	10 EB	10 EC
1	272.57	272.57	272.11	272.57
2	287.35	287.38	286.83	287.38
3	314.99	315.17	314.42	315.17

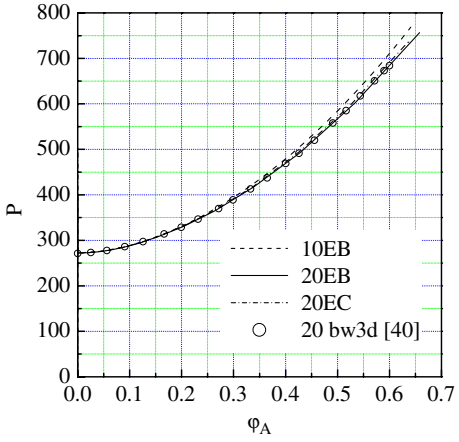

Fig. 11. Load–twist angle (middle point) curves for Example 5.

results obtained using 20 EB and EC elements are in excellent agreement with those obtained using 20 bw3d elements [40].

Example 6 (*Simply supported beam of Z-section subjected to an eccentric axial force*). This example considered is a simply supported beam of Z-section subjected to an eccentric axial force P as shown in Fig. 12. This example was analyzed by Attard [14]. The ends of the beam are free to warp and free to rotate about X_2^G and X_3^G axes, but restrained from rotation about X_1^G axis. The translation is restrained at end point A, and is free only in the direction of X_1^G axis at point B.

The present results are obtained using 40, 80 EA and 20, 40 EB elements. The linear buckling load and the nonlinear buckling load given in [14] are 88.55 kN and 119.01 kN, respectively. The present nonlinear buckling load obtained using 80 EA elements is 86.75 kN. However, no buckling load is detected for the case using EB elements. For this example, the transverse deflection and twist are initiated, regardless of the magnitude of the loading. Thus, the bifurcation buckling may be impossible. It seems that the existence of limit point on the loading–deflection curves may also be impossible for a simply supported elastic beam subjected to end axial forces. Because the higher order terms of the tangent stiffness matrix are dropped in this study, the tangent stiffness matrix used here is an approximate tangent stiffness matrix. Thus, the buckling point detected for this example may be just an artificial critical point. The load–deflection curves of the present study together with the results of [14] are shown in Figs. 13–15. The results of 20 EB elements are obtained by using 80 increments. The average number of iterations per increment is about 6. The results of 40 EB elements (not shown here) are nearly identical with those of 20 EB elements. It can be seen that the agreement is very good between the present results of 20 EB and 80 EA elements. For this example, the value of α is about 10. The discrepancy between the deflection curves of the present study and [14] is remarked when the deflections are not small. The discrepancy may be attributed at least in part to that a total Lagrangian formulation combined with the assumption of small to moderate axial displacement due to flexural deformations is used and only the terms up to the second order are retained in the derivation of the beam element in [14].

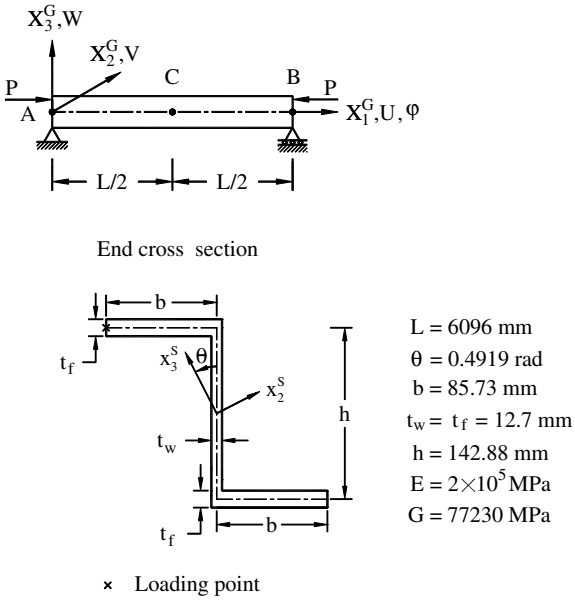

Fig. 12. Simply supported beam of Z-section subjected to an eccentric axial force (Example 6).

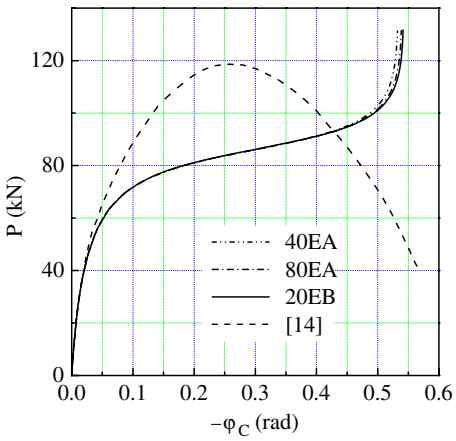

Fig. 13. Load–twist angle curves for Example 6.

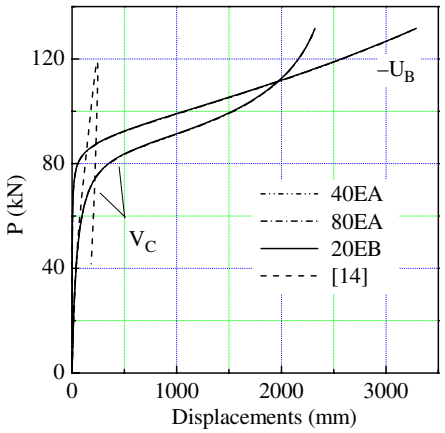

Fig. 14. Load–displacement (U_B, V_C) curves for Example 6.

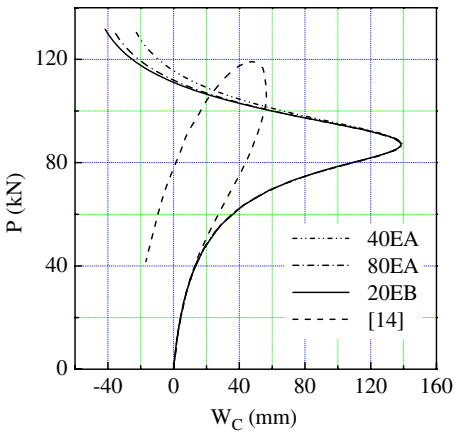

Fig. 15. Load–displacement (W_C) curves for Example 6.

Example 7 (*Cantilever beam of asymmetric angle section subjected to an eccentric axial force*). The example considered is a cantilever beam of asymmetric angle cross section subjected to an eccentric axial force P as shown in Fig. 16. This example was analyzed by Chan and Kitipornchai [17]. The clamped end of the beam is fully restrained against warping.

The value of α is about 6 for this example. The present results obtained using 10 EA, 10 EB and 20 EB elements are nearly identical. The load–deflection curves of the present study together with the results of [17] (transcribed by the authors) are shown in Fig. 17. The results of 10 EB elements are obtained by using 40 increments. The average number of iterations per increment is about 7. The discrepancy between the

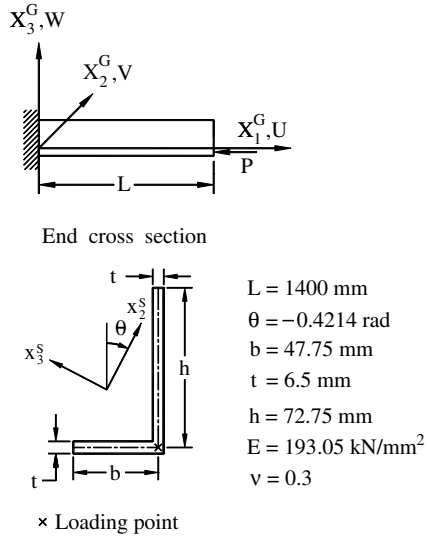

Fig. 16. Cantilever beam of asymmetric angle section subjected to an eccentric axial force (Example 7).

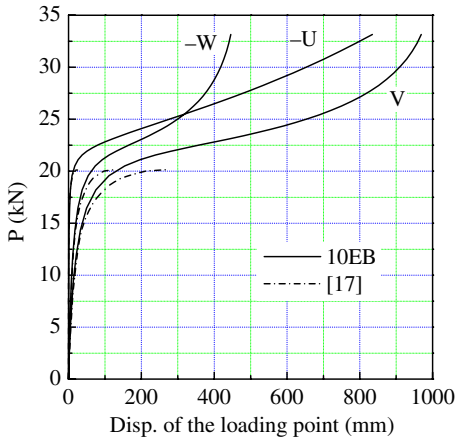

Fig. 17. Load–displacement curves for Example 7.

deflection curves of the present study and [17] is remarked when the deflections are not small. The discrepancy may be attributed at least in part to that the displacement field of elementary beam theory is used in the derivation of the beam element in [17].

Example 8 (*Cantilever beam of asymmetric channel section subjected to an axial force*). The example considered here is a cantilever beam of asymmetric channel cross-section subjected to an axial force P applied at the centroid or shear center of the end cross-section as shown in Fig. 18. The clamped end of the beam is fully restraint against warping. The directions of the X_2^G and X_3^G axes are chosen to be those of the principal centroid axes of the cross-section at the undeformed state.

The present results are obtained using 20 EB elements. The present nonlinear buckling load corresponding centroid load and the linear buckling load given in [31] are 13.991 N and 13.902 N, respectively. The load–deflection curves of the present study together with the results of [39] using 20 beam elements are shown in Fig. 19. Note that in order to compare results with those given in [39], a lateral load of $0.001P$ is applied at the centroid of the end cross-section in the direction of the X_2^G axis for the results shown in Fig. 19. It can be seen that the present results are in excellent agreement with those given in [39].

Example 9 (*Cantilever beam of asymmetric channel section subjected to an end lateral force*). The example considered here is a cantilever beam of asymmetric channel cross-section subjected to an end vertical force P as shown in Fig. 20. The clamped end of the beam is fully restraint against warping. The geometry and material properties are identical with those of Example 8. Six cases are considered. For cases (a), (b) and (c), the vertical upward load $P(+)$ is applied at the top of the web, the centroid, and the bottom of the web, respectively, and for cases (d), (e) and (f), the vertical downward load $P(-)$ is applied at the top of the web, the centroid, and the bottom of the web. The error tolerance $e_{\text{tol}} = 10^{-7}$ is used for this example. The present results are obtained using 40 EB elements. The load–deflection curves of the present study are shown in Figs. 21 and 22 for cases (a)–(f), respectively. It can be seen that the load–deflections of different loading points are similar for vertical upward load and vertical downward load, respectively.

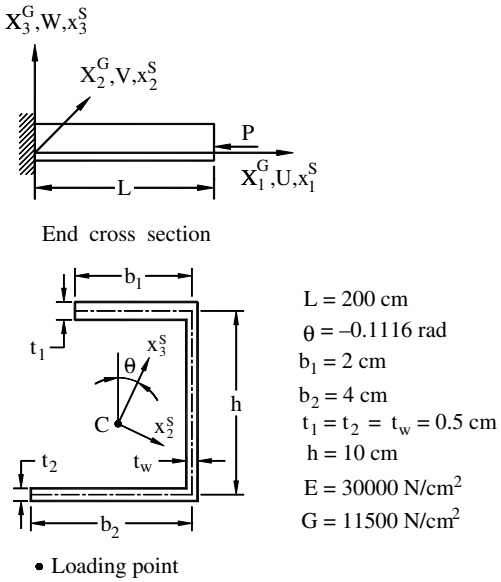

Fig. 18. Cantilever beam of asymmetric channel section subjected to an axial force (Example 8).

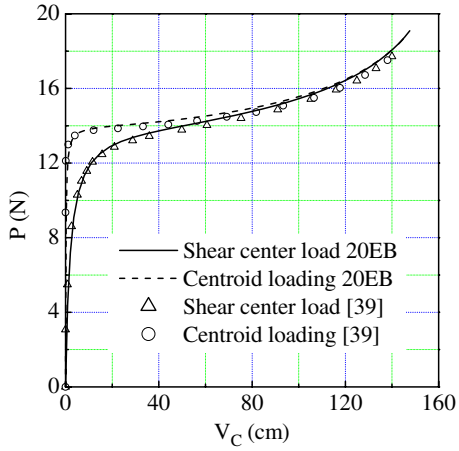

Fig. 19. Load–displacement curves for Example 8.

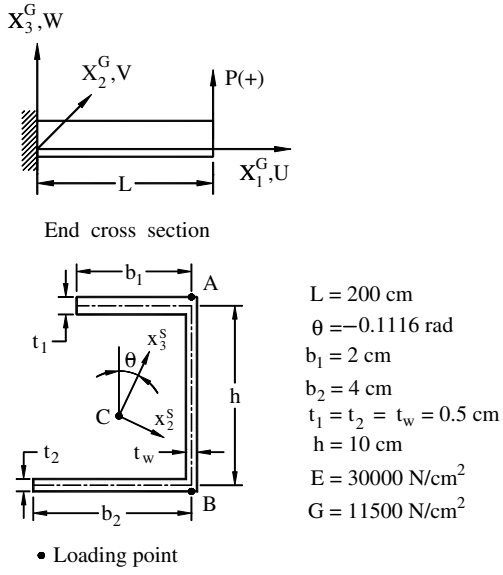

Fig. 20. Cantilever beam of asymmetric channel section subjected to a lateral end force (Example 9).

Example 10 (*Cantilever beam of Z-section subjected to an axial force at the end centroid*). The example considered here is a cantilever beam of Z-section subjected to an axial force P applied at the centroid of the end cross-section as shown in Fig. 23. The directions of the X_2^G and X_3^G axes are chosen to be those of the principal centroid axes of the cross-section at the undeformed state.

Note that because the value of warping function at the centroid of the cross-section is not zero for Z-section, a bimoment $-85.714P(\mathbf{e}_1^G \cdot \mathbf{e}_1^S)$ is induced by the axial load at the end node, where 85.714 is the

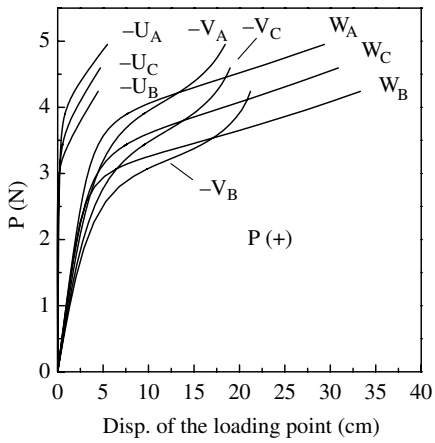

Fig. 21. Load–displacement curves for cases (a), (b) and (c) of Example 9.

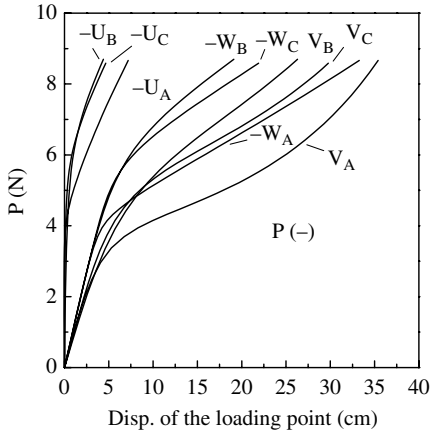

Fig. 22. Load–displacement curves for cases (d), (e) and (f) of Example 9.

value of warping function at the centroid of the cross-section, $\mathbf{e}_1^G$ and $\mathbf{e}_1^S$ are the unit vectors associated the X_1^G axis and current x_1^S axis of the end cross section. For this example, the value of α is about 9. This example is analyzed using 40, 80 EA and 20 EB elements. The results of 20 EB and 80 EA elements are nearly identical. Thus only the results of 20 EB elements are shown here. The load–deflection curves of the 20 EB elements are shown in Figs. 24–26. In Fig. 24 φ_B is the prebuckling twisting angle at node B induced by the bimoment. The present buckling load is 906.610 kN, which is in close agreement with the Euler buckling load 906.286 kN. The small discrepancy between the present buckling load and the Euler buckling load may be induced by the prebuckling twist of the cross-section. The postbuckling displacements W_B may also be attributed to the prebuckling twist of the cross-section. It can be seen from Figs. 25 and 26 that the increase of the postbuckling displacements U_B, V_B and W_B is remarked with slight increase of the applied load as expected. However, the postbuckling displacements W_B are decreased with further increase of the applied load.

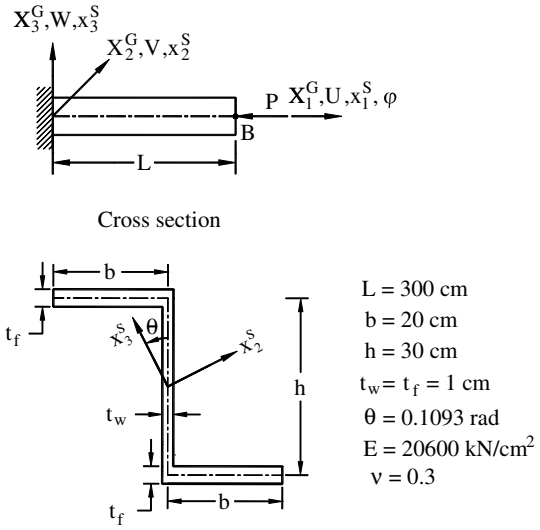

Fig. 23. Cantilever beam of Z-section subjected to an axial force at the end centroid (Example 10).

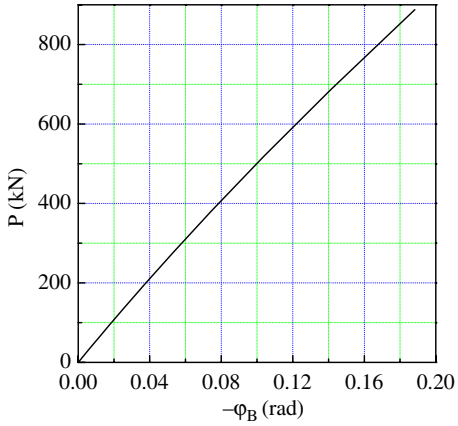

Fig. 24. Load–twist angle curve (prebuckling) for Example 10.

5. Conclusions

A consistent co-rotational total Lagrangian finite element formulation for the geometric nonlinear buckling and postbuckling analysis of thin-walled beams with generic open section is proposed. The kinematics of beam element used in [38] for monosymmetric thin-walled open-section beams is extended here. The element nodal forces are derived using the virtual work principle. The rigid body motion corresponding to the virtual nodal displacements is excluded in the derivation of the element nodal forces. A procedure based on the method described in [24] and the first order consistent linearization is proposed to determine the element coordinate system and element nodal deformations for the virtual displaced configuration corresponding to the virtual element nodal displacements. The difference between the nodal rotation parameters and the difference between the chord length of the beam element corresponding to the virtual displaced configuration and the current configuration are used as the element virtual nodal deformation displacements. All coupling among bending, twisting, and stretching deformations for beam element is considered by

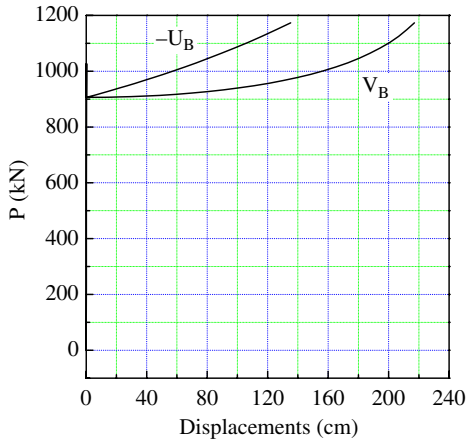

Fig. 25. Load–displacement (U_B, V_B) curves for Example 10.

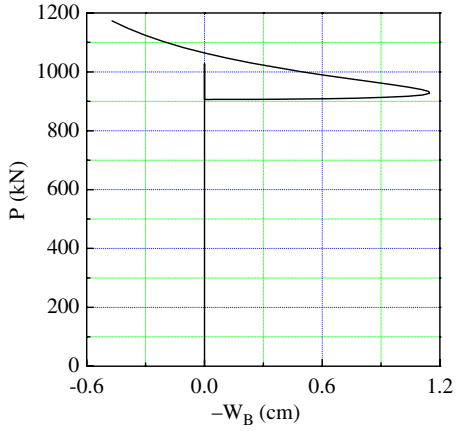

Fig. 26. Load–displacement (W_B) curves for Example 10.

consistent second-order linearization of the fully geometrically nonlinear beam theory. However, the third order term of the twist rate of the beam axis is retained in the element nodal forces. Since the rigid body motion of the element is eliminated in the consistent co-rotational formulation, there are only eight independent implicit and explicit element nodal forces. The lateral nodal force f_{ij} $(i = 2, 3, j = 1, 2)$ may be regarded as reactions to the corresponding bending moments.

It was explained that the change of element nodal forces induced by the element rigid body rotation should also be considered in the derivation of the element tangent stiffness matrix for the consistent co-rotational formulation. Thus, a stability matrix should be included in the element tangent stiffness matrix. It was demonstrated through numerical examples that the derived element tangent stiffness matrix can be used to detect different buckling loads of beam structures. Because the higher order terms of the tangent stiffness matrix are dropped, the tangent stiffness matrix used in this study is an approximate tangent stiffness matrix. Thus, the buckling points detected for Example 6, in which bifurcation buckling or snap buckling may be impossible, may be just an artificial critical point, not a bifurcation point or limit point. In order to verify the existence of bifurcation point, at the buckling point a perturbation displacement proportional to the corresponding buckling mode should be added to detect the existence of the secondary path.

In the element nodal forces and the element stiffness matrices of the present beam element and those used in [24,36–38,41], the terms relevant to the twist angle, slopes, length of the beam element will converge to zero and those relevant only to the unit extension, twist rate and curvatures of the beam element will converge to constants. The contribution of the terms relevant to the twist angle and slopes length of the beam element may be negligible with the decrease of element size. However, their convergence rates may be slower than those relevant to the unit extension, twist rate and curvatures with the decrease of element size. Thus, if the terms relevant to the twist angle, slopes, and length of the beam element are removed from the element nodal forces and the element matrices, the convergence rate of the solution may be increased. This belief was confirmed through numerical examples studied in this paper. Note that the increase of the convergent rate of solution is remarked when the ratio of the flexural stiffness between the major axis and the minor axis of the cross-section of the beam is large. Thus, it is suggested that all the underlined terms in Eqs. (34)–(39), (50), (A.3) and (B.5)–(B.9) should be removed to simplify the expression and to increase the convergence rate of solution for the present beam element. It seems that this belief can be applied to the beam elements used in [24,36–38,41] to increase the convergence rate of solution.

Acknowledgements

The authors would like to acknowledge the constructive and thoughtful comment of the referees. The research was sponsored by the national Science Council, Taiwan under the contract NSC 89-2212-E-009-052.

Appendix A. Transformation matrix $\mathbf{T}_{\theta\phi}$

The explicit form of the transformation matrix between the variation of the implicit and explicit nodal parameters may be expressed as

$$\mathbf{T}_{\theta\phi} = \mathbf{T}^0_{\theta\phi} + \mathbf{T}^1_{\theta\phi} + \mathbf{T}^2_{\theta\phi}, \tag{A.1}$$

$$\mathbf{T}^0_{\theta\phi} + \mathbf{T}^1_{\theta\phi} = \begin{bmatrix} \mathbf{0}_3 & \mathbf{0}_3 & \mathbf{0}_3 & \mathbf{0}_3 & \mathbf{0}_{3\times 2} \\ \mathbf{T}_{a1} & \mathbf{T}_{c1} & -\mathbf{T}_{a1} & \mathbf{T}_e & \mathbf{0}_{3\times 2} \\ \mathbf{T}_b & \mathbf{0}_3 & -\mathbf{T}_b & \mathbf{0}_3 & \mathbf{0}_{3\times 2} \\ \mathbf{T}_{a2} & \mathbf{T}_d & -\mathbf{T}_{a2} & \mathbf{T}_{c2} & \mathbf{0}_{3\times 2} \\ \mathbf{0}_{2\times 3} & \mathbf{0}_{2\times 3} & \mathbf{0}_{2\times 3} & \mathbf{0}_{2\times 3} & \mathbf{I}_2 \end{bmatrix}, \tag{A.2}$$

$$\mathbf{T}_{aj} = \begin{bmatrix} 0 & 0 & 0 \\ \dfrac{-\theta_{2j}}{L} & \dfrac{\theta_{11}+\theta_{12}}{2\ell} & \dfrac{-(1+\varepsilon_{0j})}{\ell} \\ \dfrac{-\theta_{3j}}{L} & \dfrac{1+\varepsilon_{0j}}{\ell} & \dfrac{\theta_{11}+\theta_{12}}{2\ell} \end{bmatrix} + (-1)^j \begin{bmatrix} 0 & \dfrac{\theta_{21}-\theta_{22}}{4\ell} & \dfrac{\theta_{31}-\theta_{32}}{4\ell} \\ 0 & -\dfrac{6y_p}{L\ell}\theta_{2j} & -\dfrac{6z_p}{L\ell}\theta_{2j} \\ 0 & -\dfrac{6y_p}{L\ell}\theta_{3j} & -\dfrac{6z_p}{L\ell}\theta_{3j} \end{bmatrix}, \tag{A.3}$$

$$\mathbf{T}_b = \begin{bmatrix} -1 & 0 & 0 \\ 0 & 0 & 0 \\ 0 & 0 & 0 \end{bmatrix},$$

$$\mathbf{T}_{cj} = \begin{bmatrix} \frac{1}{2} & \frac{\theta_{3j}}{4} & -\frac{\theta_{2j}}{4} \\ -\frac{\theta_{3j}}{2} & 1+\varepsilon_{0j} & \frac{\theta_{11}+\theta_{12}}{2} \\ \frac{\theta_{2j}}{2} & -\frac{(\theta_{11}+\theta_{12})}{2} & 1+\varepsilon_{0j} \end{bmatrix} + (-1)^j \begin{bmatrix} 0 & 0 & 0 \\ 0 & \frac{3z_p}{L}\theta_{2j} & -\frac{3y_p}{L}\theta_{2j} \\ 0 & \frac{3z_p}{L}\theta_{3j} & -\frac{3y_p}{L}\theta_{3j} \end{bmatrix},$$

$$\mathbf{T}_d = \begin{bmatrix} -\frac{1}{2} & -\frac{\theta_{31}}{4} & \frac{\theta_{21}}{4} \\ \frac{\theta_{32}}{2} & \frac{3z_p}{L}\theta_{22} & -\frac{3y_p}{L}\theta_{22} \\ -\frac{\theta_{22}}{2} & \frac{3z_p}{L}\theta_{32} & -\frac{3y_p}{L}\theta_{32} \end{bmatrix}, \quad \mathbf{T}_e = \begin{bmatrix} -\frac{1}{2} & -\frac{\theta_{32}}{4} & \frac{\theta_{22}}{4} \\ \frac{\theta_{31}}{2} & -\frac{3z_p}{L}\theta_{21} & \frac{3y_p}{L}\theta_{21} \\ -\frac{\theta_{21}}{2} & -\frac{3z_p}{L}\theta_{31} & \frac{3y_p}{L}\theta_{31} \end{bmatrix},$$

$$\mathbf{T}^2_{\theta\phi} = \begin{bmatrix} \mathbf{0}_3 & \mathbf{0}_3 & \mathbf{0}_3 & \mathbf{0}_3 & \mathbf{0}_{3\times 2} \\ \mathbf{T}_{A1} & \mathbf{T}_{B1} & -\mathbf{T}_{A1} & \mathbf{T}_{C1} & \mathbf{0}_{3\times 2} \\ \mathbf{0}_3 & \mathbf{0}_3 & \mathbf{0}_3 & \mathbf{0}_3 & \mathbf{0}_{3\times 2} \\ \mathbf{T}_{A2} & \mathbf{T}_{B2} & -\mathbf{T}_{A2} & \mathbf{T}_{C2} & \mathbf{0}_{3\times 2} \\ \mathbf{0}_{2\times 3} & \mathbf{0}_{2\times 3} & \mathbf{0}_{2\times 3} & \mathbf{0}_{2\times 3} & \mathbf{0}_{2\times 2} \end{bmatrix}, \tag{A.4}$$

$$\mathbf{T}_{Aj} = \begin{bmatrix} 0 & 0 & 0 \\ 0 & (G_{b2}+G_{b4})\frac{\theta_{2j}}{\ell} & -(G_{c2}+G_{c4})\frac{\theta_{2j}}{\ell} \\ 0 & (G_{b2}+G_{b4})\frac{\theta_{3j}}{\ell} & -(G_{c2}+G_{c4})\frac{\theta_{3j}}{\ell} \end{bmatrix}, \tag{A.5}$$

$$\mathbf{T}_{Bj} = \begin{bmatrix} 0 & 0 & 0 \\ 0 & G_{c2}\theta_{2j} & G_{b2}\theta_{2j} \\ 0 & G_{c2}\theta_{3j} & G_{b2}\theta_{3j} \end{bmatrix}, \quad \mathbf{T}_{Cj} = \begin{bmatrix} 0 & 0 & 0 \\ 0 & G_{c4}\theta_{2j} & G_{b4}\theta_{2j} \\ 0 & G_{c4}\theta_{3j} & G_{b4}\theta_{3j} \end{bmatrix},$$

where $\mathbf{T}^i_{\theta\phi}$ $(i=0,1,2)$ are the ith order terms of $\mathbf{T}_{\theta\phi}$, $\mathbf{I}_2$ is the identity matrices of order 2×2, $\mathbf{0}_2$, $\mathbf{0}_3$, $\mathbf{0}_{2\times 3}$ and $\mathbf{0}_{3\times 2}$ are zero matrices of order 2×2, 3×3, 3×2 and 2×3, respectively, ε_{0j} $(j=1,2)$ are the nodal value of ε_0 at node j, and G_{bi} and G_{ci} $(i=2,4)$ are the ith element of column matrices $\mathbf{G}_b$ and $\mathbf{G}_c$ given in Eq. (39), respectively.

Appendix B. Relations between the explicit and implicit element nodal forces

$$f_{12} = -f_{11} = f^{\theta}_{12} + f^{\theta\phi}_{12}, \tag{B.1}$$

$$f^{\theta\phi}_{12} = \frac{\theta_{21}}{L}m^{\theta}_{21} + \frac{\theta_{22}}{L}m^{\theta}_{22} + \frac{\theta_{31}}{L}m^{\theta}_{31} + \frac{\theta_{32}}{L}m^{\theta}_{32}, \tag{B.2}$$

$$f_{21} = -f_{22} = \frac{1}{\ell}(m_{31}+m_{32}), \tag{B.3}$$

$$f_{31} = -f_{32} = -\frac{1}{\ell}(m_{21}+m_{22}), \tag{B.4}$$

$$m_{11} = -m_{12} = \frac{1}{2}(m^{\theta}_{11} - m^{\theta}_{12}) + \underline{\frac{1}{2}\theta_{32}m^{\theta}_{22}} - \underline{\frac{1}{2}\theta_{31}m^{\theta}_{21}} - \underline{\frac{1}{2}\theta_{22}m^{\theta}_{32}} + \underline{\frac{1}{2}\theta_{21}m^{\theta}_{31}}, \tag{B.5}$$

$$m_{21} = (1+\varepsilon_{0j})m^{\theta}_{21} + \underline{\frac{\theta_{31}}{4}(m^{\theta}_{11} - m^{\theta}_{12})} - \frac{(\theta_{11}+\theta_{12})}{2}m^{\theta}_{31} - \frac{3z_p}{L}(m^{\theta}_{21}\theta_{21} - m^{\theta}_{22}\theta_{22}) - \frac{3z_p}{L}(m^{\theta}_{31}\theta_{31} - m^{\theta}_{32}\theta_{32}) + \underline{f^{\theta\phi}_{12}G_{c2}L}, \tag{B.6}$$

$$m_{31} = (1+\varepsilon_{0j})m^{\theta}_{31} - \underline{\frac{\theta_{21}}{4}(m^{\theta}_{11} - m^{\theta}_{12})} + \frac{(\theta_{11}+\theta_{12})}{2}m^{\theta}_{21} + \frac{3y_p}{L}(m^{\theta}_{21}\theta_{21} - m^{\theta}_{22}\theta_{22}) + \frac{3y_p}{L}(m^{\theta}_{31}\theta_{31} - m^{\theta}_{32}\theta_{32}) + \underline{f^{\theta\phi}_{12}G_{b2}L}, \tag{B.7}$$

$$m_{22} = (1+\varepsilon_{0j})m^{\theta}_{22} - \underline{\frac{\theta_{32}}{4}(m^{\theta}_{11} - m^{\theta}_{12})} - \frac{(\theta_{11}+\theta_{12})}{2}m^{\theta}_{32} - \frac{3z_p}{L}(m^{\theta}_{21}\theta_{21} - m^{\theta}_{22}\theta_{22}) - \frac{3z_p}{L}(m^{\theta}_{31}\theta_{31} - m^{\theta}_{32}\theta_{32}) + \underline{f^{\theta\phi}_{12}G_{c4}L}, \tag{B.8}$$

$$m_{32} = (1+\varepsilon_{0j})m^{\theta}_{32} + \underline{\frac{\theta_{22}}{4}(m^{\theta}_{11} - m^{\theta}_{12})} + \frac{(\theta_{11}+\theta_{12})}{2}m^{\theta}_{22} + \frac{3y_p}{L}(m^{\theta}_{21}\theta_{21} - m^{\theta}_{22}\theta_{22}) + \frac{3y_p}{L}(m^{\theta}_{31}\theta_{31} - m^{\theta}_{32}\theta_{32}) + \underline{f^{\theta\phi}_{12}G_{b4}L}. \tag{B.9}$$

Note that the above underlined terms will converge to zero with the decrease of the element size and the value of $\theta_{11}+\theta_{12}$ in Eqs. (B.6)–(B.9) is equal to zero. Bimoment B_j $(j=1,2)$ are identical for the explicit and implicit element nodal forces. As expected, there are only eight independent explicit element nodal forces. The final forms of f_{ij} $(i=2,3, j=1,2)$ in Eqs. (B.3) and (B.4) may be regarded as reactions to the corresponding bending moments.

Appendix C. The matrix $\mathbf{H}_R$

$$\mathbf{H}_R = \begin{bmatrix} \mathbf{h}^a_{R1} & \mathbf{h}^c_{R1} & -\mathbf{h}^a_{R1} & \mathbf{h}^c_{R1} & \mathbf{0}_{3\times2} \\ \mathbf{h}^b_{R1} & \mathbf{h}^d_{R1} & -\mathbf{h}^b_{R1} & \mathbf{h}^d_{R1} & \mathbf{0}_{3\times2} \\ \mathbf{h}^a_{R2} & \mathbf{h}^c_{R2} & -\mathbf{h}^a_{R2} & \mathbf{h}^c_{R2} & \mathbf{0}_{3\times2} \\ \mathbf{h}^b_{R2} & \mathbf{h}^d_{R2} & -\mathbf{h}^b_{R2} & \mathbf{h}^d_{R2} & \mathbf{0}_{3\times2} \\ \mathbf{0}_{2\times3} & \mathbf{0}_{2\times3} & \mathbf{0}_{2\times3} & \mathbf{0}_{2\times3} & \mathbf{0}_2 \end{bmatrix},$$

$$\mathbf{h}^a_{Rj} = \begin{bmatrix} 0 & \frac{f_{2j}}{\ell} & \frac{f_{3j}}{\ell} \\ 0 & -\frac{f_{1j}}{\ell} & 0 \\ 0 & 0 & -\frac{f_{1j}}{\ell} \end{bmatrix}, \quad \mathbf{h}^b_{Rj} = \begin{bmatrix} 0 & \frac{m_{2j}}{\ell} & \frac{m_{3j}}{\ell} \\ 0 & -\frac{m_{1j}}{\ell} & 0 \\ 0 & 0 & -\frac{m_{1j}}{\ell} \end{bmatrix},$$

$$\mathbf{h}^c_{Rj} = \begin{bmatrix} 0 & 0 & 0 \\ -\frac{f_{3j}}{2} & 0 & 0 \\ \frac{f_{2j}}{2} & 0 & 0 \end{bmatrix}, \quad \mathbf{h}^d_{Rj} = \begin{bmatrix} 0 & 0 & 0 \\ -\frac{m_{3j}}{2} & 0 & 0 \\ \frac{m_{2j}}{2} & 0 & 0 \end{bmatrix},$$

in which $j=1,2$, $\mathbf{0}_2$, $\mathbf{0}_{2\times3}$ and $\mathbf{0}_{3\times2}$ are zero matrices of order 2×2, 3×2 and 2×3, respectively.

Appendix D. The matrix $\mathbf{H}_{\theta}$

$$\mathbf{H}_{\theta}=\begin{bmatrix}\mathbf{0}_3 & \mathbf{h}_{a1} & \mathbf{0}_3 & \mathbf{h}_{a2} & \mathbf{0}_{3\times2}\\ \mathbf{h}_{b1}^t & \mathbf{h}_{d1} & -\mathbf{h}_{b1}^t & \mathbf{h}_e & \mathbf{0}_{3\times2}\\ \mathbf{0}_3 & -\mathbf{h}_{a1} & \mathbf{0}_3 & -\mathbf{h}_{a2} & \mathbf{0}_{3\times2}\\ \mathbf{h}_{b2}^t & \mathbf{h}_e^t & -\mathbf{h}_{b2}^t & \mathbf{h}_{d2} & \mathbf{0}_{3\times2}\\ \mathbf{0}_{2\times3} & \mathbf{0}_{2\times3} & \mathbf{0}_{2\times3} & \mathbf{0}_{2\times3} & \mathbf{0}_2\end{bmatrix},$$

$$\mathbf{h}_{aj}=\begin{bmatrix}0 & 0 & 0\\ \dfrac{m_{21}^{\theta1}+m_{22}^{\theta1}}{2\ell} & 0 & 0\\ \dfrac{m_{31}^{\theta1}+m_{32}^{\theta2}}{2\ell} & 0 & 0\end{bmatrix}+(-1)^j\begin{bmatrix}0 & 0 & 0\\ 0 & \dfrac{m_{11}^{\theta1}-m_{12}^{\theta1}}{4\ell} & 0\\ 0 & 0 & \dfrac{m_{11}^{\theta1}-m_{12}^{\theta1}}{4\ell}\end{bmatrix}$$
$$+\begin{bmatrix}0 & -\dfrac{m_{2j}^{\theta1}}{L} & -\dfrac{m_{3j}^{\theta1}}{L}\\ 0 & 0 & 0\\ 0 & 0 & 0\end{bmatrix}+(-1)^j\begin{bmatrix}0 & 0 & 0\\ 0 & -\dfrac{6y_p}{L\ell}m_{2j}^{\theta1} & -\dfrac{6y_p}{L\ell}m_{3j}^{\theta1}\\ 0 & -\dfrac{6z_p}{L\ell}m_{2j}^{\theta1} & -\dfrac{6z_p}{L\ell}m_{3j}^{\theta1}\end{bmatrix},$$

$$\mathbf{h}_{bj}=\begin{bmatrix}0 & -\dfrac{m_{2j}^{\theta1}}{L} & -\dfrac{m_{3j}^{\theta1}}{L}\\ 0 & 0 & 0\\ 0 & 0 & 0\end{bmatrix}+(-1)^j\begin{bmatrix}0 & 0 & 0\\ 0 & -\dfrac{6y_p}{L^2}m_{2j}^{\theta1} & -\dfrac{6y_p}{L^2}m_{3j}^{\theta1}\\ 0 & -\dfrac{6z_p}{L^2}m_{2j}^{\theta1} & -\dfrac{6z_p}{L^2}m_{3j}^{\theta1}\end{bmatrix},$$

$$\mathbf{h}_{dj}=\begin{bmatrix}0 & \dfrac{m_{3j}^{\theta1}}{2} & -\dfrac{m_{2j}^{\theta1}}{2}\\ -\dfrac{m_{3j}^{\theta1}}{2} & 0 & 0\\ \dfrac{m_{2j}^{\theta1}}{2} & 0 & 0\end{bmatrix}+(-1)^j\begin{bmatrix}0 & 0 & 0\\ 0 & 0 & \dfrac{m_{12}^{\theta1}-m_{11}^{\theta1}}{4}\\ 0 & \dfrac{m_{11}^{\theta1}-m_{12}^{\theta1}}{4} & 0\end{bmatrix}$$
$$+(-1)^j\begin{bmatrix}0 & 0 & 0\\ 0 & \dfrac{6z_p}{L}m_{2j}^{\theta1} & \dfrac{3z_p}{L}m_{3j}^{\theta1}-\dfrac{3y_p}{L}m_{2j}^{\theta1}\\ 0 & \dfrac{3z_p}{L}m_{3j}^{\theta1}-\dfrac{3y_p}{L}m_{2j}^{\theta1} & -\dfrac{6y_p}{L}m_{3j}^{\theta1}\end{bmatrix},$$

$$\mathbf{h}_e=\begin{bmatrix}0 & -\dfrac{m_{32}^{\theta1}}{2} & \dfrac{m_{22}^{\theta1}}{2}\\ -\dfrac{m_{31}^{\theta1}}{2} & 0 & 0\\ \dfrac{m_{21}^{\theta1}}{2} & 0 & 0\end{bmatrix}+\begin{bmatrix}0 & 0 & 0\\ 0 & \dfrac{3z_p}{L}(m_{22}^{\theta1}-m_{21}^{\theta1}) & \dfrac{3y_p}{L}m_{21}^{\theta1}+\dfrac{3z_p}{L}m_{32}^{\theta1}\\ 0 & -\dfrac{3y_p}{L}m_{22}^{\theta1}-\dfrac{3z_p}{L}m_{31}^{\theta1} & \dfrac{3y_p}{L}(m_{31}^{\theta1}-m_{32}^{\theta1})\end{bmatrix},$$

where $m_{ij}^{\theta1}$ $(i=1,2,3,j=1,2)$ are the first order terms of m_{ij}^{θ}, $\mathbf{0}_2$, $\mathbf{0}_3$, $\mathbf{0}_{2\times3}$ and $\mathbf{0}_{3\times2}$ are zero matrices of order 2×2, 3×3, 3×2 and 2×3, respectively.

References

[1] H.L. Engel, J.N. Goodier, Measurements of torsional stiffness changes and instability due to tension, compression and bending, J. Appl. Mech. ASME (1953) 553–560.
[2] M. Gregory, A nonlinear bending effect when certain unsymmetrical sections are subjected to a pure torque, Aust. J. Appl. Sci. 11 (1960) 33–48.
[3] V.Z. Vlasov, Thin Walled Elastic Beams, second ed. (English translation published for US Science Foundation by Israel Program for Scientific Translations), 1961.
[4] S.P. Timoshenko, J.M. Gere, Theory of Elastic Stability, second ed., McGraw-Hill, NY, 1963.
[5] R.S. Barsoum, R.H. Gallagher, Finite element analysis of torsional and torsional-flexural stability problems, moments, Int. J. Numer. Methods Engrg. 2 (1970) 335–352.
[6] J.M. Anderson, N.S. Trahair, Stability of monosymmetric beams and cantilevers, J. Struct. Div. ASCE 98 (1972) 269–286.
[7] S.T. Woolcock, N.S. Trahair, Post-buckling behavior of determinate beams, J. Engrg. Mech. Div. ASCE 100 (1974) 151–171.
[8] D.O. Brush, B.O. Almroth, Buckling of Bars, Plates and Shells, McGraw-Hill, NY, 1975.
[9] H. Ziegler, Principles of Structural Stability, Birkhauser Verlag, Basel, 1977.
[10] J.H. Argyris, P.C. Dunne, D.W. Scharpf, On large displacement-small strain analysis of structures with rotation degree of freedom, Comput. Methods Appl. Mech. Engrg. 14 (1978) 401–451;
J.H Argyris, P.C. Dunne, D.W. Scharpf, Comput. Methods Appl. Mech. Engrg. 15 (1978) 99–135.
[11] J.H. Argyris, O. Hilpert, G.A. Malejannakis, D.W. Scharpf, On the geometrical stiffness of a beam in space—a consistent v.w. approach, Comput. Methods Appl. Mech. Engrg. 20 (1979) 105–131.
[12] J.H. Argyris, H. Balmer, J.St. Doltsinis, P.C. Dunne, M. Haase, M. Kleiber, G.A. Malejannakis, H.P. Mlejenek, M. Muller, D.W. Scharpf, Finite element method—the natural approach, Comput. Methods Appl. Mech. Engrg. 17–18 (1979) 1–106.
[13] A. Gjelsvik, The Theory of Thin Walled Bars, John Wiley & Sons, NY, 1981.
[14] M.M. Attard, The elastic flexural-torsional response of thin-walled open beams, Ph.D. thesis, University of New South Wales, Australia, 1984.
[15] M.M. Attard, Lateral buckling analysis of beams by FEM, Comput. Struct. 23 (1986) 217–231.
[16] J.C. Simo, L. Vu-Quoc, A three-dimensional finite strain rod model. Part II: Computational aspects, Comput. Methods Appl. Mech. Engrg. 58 (1986) 79–116.
[17] S.L. Chan, S. Kitipornchai, Geometrically nonlinear analysis of asymmetrical thin-walled beam-columns, Engrg. Struct. 9 (1987) 243–254.
[18] N.G.R. Iyengar, Structural Stability of Columns and Plates, Ellis Horwood, UK, 1988.
[19] W.F. Chen, E.M. Lui, Structural Stability, Theory and Implementation, Elsevier Science Publishing Co., Inc., NY, 1988.
[20] A. Cardona, M. Geradin, A beam finite element non-linear theory with finite rotations, Int. J. Numer. Methods Engrg. 26 (1988) 2403–2438.
[21] M. Iura, S.N. Atluri, On a consistent theory and variational formulation of finitely stretched and rotated 3-D spaced-curved beams, Comput. Mech. 4 (1989) 73–88.
[22] M.A. Crisfield, A consistent co-rotational formulation for non-linear, three-dimensional, beam elements, Comput. Methods Appl. Mech. Engrg. 81 (1990) 131–150.
[23] H. Chen, G.E. Blandford, Thin-walled space frames, Part I: large deformation analysis theory, and Part II: algorithmic details and applications, J. Struct. Engrg. ASCE 117 (1991) 2499–2539.
[24] K.M. Hsiao, Corotational total Lagrangian formulation for three-dimensional beam element, AIAA J. 30 (1992) 797–804.
[25] Y.L. Pi, N.S. Trahair, Prebuckling deflections and lateral buckling: Part I: theory and Part II: application, J. Struct. Engrg. ASCE 118 (1992) 2949–2985.
[26] A.S. Gendy, A.F. Saleeb, Generalized mixed finite element model for pre- and post-quasistatic buckling response of thin-walled framed structures, Int. J. Numer. Methods Engrg. 37 (1994) 297–322.
[27] B.A. Izzuddin, An Eulerian approach to the large displacement analysis of thin-walled frames, Proc. Inst. Civ. Engrs. Struct. Bldgs. 110 (1995) 50–65.
[28] G. Jelenic, M. Saje, A kinematically exact space finite strain beam model-finite element formulation by generalized virtual work principle, Comput. Methods Appl. Mech. Engrg. 120 (1995) 131–161.
[29] B.A. Izzuddin, D.L. Smith, Large-displacement analysis of elastoplastic thin-walled frames. Part I: formulation and implementation and Part II: verification and application, J. Struct. Engrg. ASCE 122 (1996) 905–925.
[30] A. Ibrahimbegovic, H. Shakourzadeh, J.L. Batoz, M.A. Mikdad, Y.Q. Gao, On the role of geometrically exact and second-order theories in buckling and post-buckling analysis of three-dimensional beam structures, Comput. Struct. 61 (1996) 1101–1114.
[31] M.Y. Kim, S.P. Chang, S.B. Kim, Spatial stability analysis of thin walled space frames, Int. J. Numer. Methods Engrg. 39 (1996) 499–525.
[32] Y. Goto, X.S. Li, T. Kasugal, Buckling analysis of elastic space rods under torsional moment, J. Engrg. Mech. ASCE 122 (1996) 826–833.

[33] K.M. Hsiao, R.T. Yang, W.Y. Lin, A consistent finite element formulation for linear buckling analysis of spatial beams, Comput. Methods Appl. Mech. Engrg. 156 (1998) 259–276.
[34] L.H. Teh, M.J. Clarke, Co-rotational and Lagrangian formulations for elastic three-dimensional beam finite elements, J. Construct. Steel Res. 48 (1998) 123–144.
[35] F. Gruttmann, R. Sauer, W. Wagner, A geometrical nonlinear eccentric 3D-beam element with arbitrary cross-sections, Comput. Methods Appl. Mech. Engrg. 160 (1998) 383–400.
[36] K.M. Hsiao, W.Y. Lin, A co-rotational finite element formulation for buckling and postbuckling analysis of spatial beams, Comput. Methods Appl. Mech. Engrg. 188 (2000) 567–594.
[37] W.Y. Lin, K.M. Hsiao, Co-rotational formulation for geometric nonlinear analysis of doubly symmetric thin-walled beams, Comput. Methods Appl. Mech. Engrg. 190 (2001) 6023–6052.
[38] K.M. Hsiao, W.Y. Lin, A co-rotational formulation for thin-walled beams with monosymmetric open section, Comput. Methods Appl. Mech. Engrg. 190 (2000) 1163–1185.
[39] M.Y. Kim, S.P. Chang, S.B. Kim, Postbuckling analysis of nonsymmetric thin-walled frames, Part I: theoretical considerations based on semitangential property, and Part II: geometrically nonlinear FE procedure, J. Engrg. Mech. ASCE 127 (2001) 769–790.
[40] J.-M. Battin, C. Pacoste, Co-rotational beam elements with warping effects in instability problems, Comput. Methods Appl. Mech. Engrg. 191 (2002) 1755–1789.
[41] W.Y. Lin, K.M. Hsiao, A buckling and postbuckling analysis of rods under end torque and compressive load, Comput. Model. Engrg. Sci. 4 (2003) 259–271.
[42] D. Zupan, M. Saje, Finite element formulation of geometrically exact three-dimensional beam theories based on interpolation of strain measurements, Comput. Methods Appl. Mech. Engrg. 192 (2003) 5209–5248.
[43] K. Mattiasson, A. Samuelsson, Total and updated Lagrangian forms of the co-rotational finite element formulation in geometrically and materially nonlinear analysis, in: C. Tailor, E. Hinton, D.R.J. Owen (Eds.), Numerical Methods for Non-linear Problems, vol. 2, Pineridge Press, Swansea, UK, 1984, pp. 135–151.
[44] J.C. Simo, L. Vu-Quoc, The role of non-linear theories in transient dynamic analysis of flexible structures, J. Sound Vib. 119 (1987) 487–508.
[45] R.D. Cook, W.C. Young, Advanced Mechanics of Materials, Macmillan Publishing Company, NY, 1985.
[46] S. Timoshenko, Strength of Materials, Prat II: Advanced Theory and Problems, D. Van Nostrand, Princeton, NJ, 1956.
[47] H. Goldstein, Classical Mechanics, Addision-Wesley, Reading, MA, 1980.
[48] T.J. Chung, Continuum Mechanics, Prentice-Hall, NJ, 1988.
[49] K.S. Schweizerhof, E. Ramm, Displacement dependent pressure loads in nonlinear finite element analysis, Comput. Struct. 18 (1984) 1099–1114.
[50] C.C. Rankin, B. Nour-Omid, The use of projectors to improve finite element performance, Comput. Struct. 30 (1988) 257–267.
[51] B. Nour-Omid, C.C. Rankin, Finite rotation analysis and consistent linearization using projectors, Comput. Methods Appl. Mech. Engrg. 93 (1991) 353–384.
[52] M.A. Crisfield, A fast incremental/iterative solution procedure that handles 'snap through', Comput. Struct. 13 (1981) 55–62.
[53] K.M. Hsiao, C.M. Tsay, A motion process for large displacement analysis of spatial frames, Int. J. Space Struct. 6 (1991) 133–139.
[54] T. Matsui, O. Matsuoka, A new finite element scheme for instability analysis of thin shells, Int. J. Numer. Methods Engrg. 10 (1976) 145–170.
[55] Y. Goto, Y. Watanabe, T. Kasugai, M. Obata, Elastic buckling phenomenon applicable to deployable rings, Int. J. Solids Struct. 29 (1992) 893–909.